

Electrospinning-Based Strategies for Battery Materials

Xiaoyan Li, Weichen Chen, Qingrong Qian, Haitao Huang, Yuming Chen,*
Ziqiang Wang,* Qinghua Chen,* Jing Yang,* Ju Li,* and Yiu-Wing Mai*

In honor of John B Goodenough

Electrospinning is a popular technique to prepare 1D tubular/fibrous nanomaterials that assemble into 2D/3D architectures. When combined with other material processing techniques such as chemical vapor deposition and hydrothermal treatment, electrospinning enables powerful synthesis strategies that can tailor structural and compositional features of energy storage materials. Herein, a simple description is given of the basic electrospinning technique and its combination with other synthetic approaches. Then its employment in the preparation of frameworks and scaffolds with various functions is introduced, e.g., a graphitic tubular network to enhance the electronic conductivity and structural integrity of the electrodes. Current developments in 3D scaffold structures as a host for Li metal anodes, sulfur cathodes, membrane separators, or as a 3D matrix for polymeric solid-state electrolytes for rechargeable batteries are presented. The use of 1D electrospun nanomaterials as a nanoreactor for in situ transmission electron microscopy (TEM) observations of the mechanisms of materials synthesis and electrochemical reactions is summarized, which has gained popularity due to easy mechanical manipulation, electron transparency, electronic conductivity, and the easy prepositioning of complex chemical ingredients by liquid-solution processing. Finally, an outlook on industrial production and future challenges for energy storage materials is given.

1. Introduction

Energy storage systems such as lithium-ion batteries (LIBs), lithium–sulfur (Li–S) batteries, and solid-state alkali-metal batteries are considered as the most promising power sources for portable devices and electric vehicles (EVs) (Figure 1b).^[1] With the fast-growing demands in electronic devices and EVs, it is urgent to develop next-generation batteries with long cycle life and high energy density.^[2] The bottlenecks of energy storage systems include structural instability, sluggish redox kinetics, and loss of electronic conductivity and active materials, leading to short cycling life and low energy density.^[3] For example, high-capacity anode materials suffer from large volume change up to 400% during cycling, resulting in structural instability and electronic and ionic transport degradation.^[4] As another example, the main problem in Li–S batteries is the sulfur cathode with the issues of nonconductivity and dissolved polysulfides upon cycling, causing low capacity

Prof. X. Y. Li, Prof. Q. R. Qian, Dr. Y. M. Chen, Prof. Q. H. Chen
College of Environmental Science and Engineering
Fujian Normal University
Fuzhou 350007, China
E-mail: yumingc126@126.com, yumingc@mit.edu; cqhuar@126.com

Prof. H. T. Huang
Department of Applied Physics
The Hong Kong Polytechnic University
Hong Kong, China

W. C. Chen
School of Energy and Chemical Engineering
Xiamen University Malaysia
Darul Ehsan, Sepang, Selangor 43900, Malaysia

Dr. Y. M. Chen, Dr. Z. Q. Wang, Prof. J. Li
Department of Nuclear Science and Engineering and Department of
Materials Science and Engineering
Massachusetts Institute of Technology
Cambridge, MA 02139, USA
E-mail: wzq8624@126.com; liju@mit.edu

Prof. Q. H. Chen
Fujian Polytechnic Normal University
Fuqing, Fujian Province 350300, China

Dr. J. Yang
Department of Chemical Engineering
Massachusetts Institute of Technology
Cambridge, MA 02139, USA
E-mail: jyangzt@mit.edu

Prof. Y.-W. Mai
Centre for Advanced Materials Technology (CAMT)
School of Aerospace
Mechanical and Mechatronics Engineering J07
The University of Sydney
Sydney, NSW 2006, Australia
E-mail: yiu-wing.mai@sydney.edu.au

 The ORCID identification number(s) for the author(s) of this article can be found under <https://doi.org/10.1002/aenm.202000845>.

DOI: 10.1002/aenm.202000845

and short cycle life.^[5] 80% volume change of sulfur upon cycling exacerbates the problem.^[6] For solid-state alkali-metal batteries, although polymeric solid-state electrolytes (SEs) show good contact with alkali metal, their low ionic conductivity yields low rate capability of batteries.^[7]

The performance of these energy storage systems depends significantly on the characteristics of the electrode.^[8] Generally, the electrode, which is a composite material, should maintain structural stability of the components upon cycling to obtain long cycle life.^[9] Also, the electrode should possess proper porous architecture to promote dual transport of alkali-metal ions and free electrons.^[10] Hence, the development of synthetic techniques to enable the electrode materials with tailored structure, morphology and composition is critical for high-performance energy storage materials.^[11] 1D nanostructured hybrid electrodes have been developed to tackle these problems in various energy storage systems.^[12] Electrospinning is a cheap and easily tunable synthetic technique to create 1D fibers (with multiple embedded phases) that can assemble into 2D or 3D architectures.^[13] Further, when combining with other means, such as CVD, carbothermal reduction of metal (Ni⁰) particles and their migration and etching, and hydrothermal method, electrospinning enables a powerful strategy to tailor the structural and compositional features of energy storage materials.^[14] 1D nanomaterials synthesized via the combined approaches can also work as nanoreactors for in situ transmission electron microscopy (TEM) observations to characterize the mechanisms of the materials synthesis process and electrochemical reaction behaviors.^[15]

2. Electrospinning and Associated Synthetic Methods

Electrospinning technology has received increasing attention, especially from the nanomaterials community. It is one of the simplest and most effective methods to synthesize 1D nanostructured fibers with diameter ranging from few nanometers up to micrometers.^[16] As shown in Figure 1a, an electrospinning setup is generally composed of a high voltage power supply (1–100 kV), a spinneret with a hollow needle nozzle (inner diameter of 0.1–1.0 mm) and a metallic collector (rotating drum, shifting plate, etc.). The electrospinning process can be divided into three steps. First, the surface of an electrically conductive polymer solution (or melt) is charged when a high electrical potential is applied between a collector and a spinneret separated by distance h (about of 20 cm). A liquid tip with a conical shape called the Taylor cone will be formed due to the electrostatic forces that deviates from the spherical tip shape demanded by the surface tension alone. Second, a charged jet will be ejected from the spinneret tip when the electrostatic force overcomes the surface tension of the liquid. And then the charged jet in free flight experiences a complex bending, stretching and whipping motion due to the repulsive forces between the surface charges carried to form a long thread. Third, the jet will further elongate and become thinner, accompanied by the evaporation of the solvent therein; the solidified nanofibers will form and finally gather on the collector within a collection diameter D (same order as $h \approx 20$ cm since the flying fibers are confined in a big-cone shaped 3D envelop shown in Figure 1a). The electrospinning technique was first exploited to



Xiaoyan Li received her Ph.D. in 2015 from The Hong Kong Polytechnic University under Prof. Haitao Huang, Prof. Yiu-Wing Mai and Prof. Limin Zhou. During her PhD program, she worked with Prof. Xiaodong Chen in Nanyang Technological University as a visiting student. She received the Award Program for Minjiang Scholar Professorship. Her research

interests mainly focus on electrospinning, environment-friendly materials, and energy storage.



Yuming Chen received his Ph.D. in 2014 from The Hong Kong Polytechnic University under Prof. Yiu-Wing Mai and Prof. Limin Zhou. During his Ph.D. program, he worked with Prof. John B Goodenough in The University of Texas at Austin in 2013 as a visiting student. His research interests include electrospinning, in situ TEM, and energy storage.



Yiu-Wing Mai is University Professor in Mechanical Engineering at the University of Sydney. He obtained his Ph.D. on fracture mechanics from the University of Hong Kong and pursued postdoctoral research at the University of Michigan and Imperial College London. His current interest is on multifunctional polymer nanocomposites. He is a

fellow of the Royal Society and a foreign member of the Chinese Academy of Engineering.

produce polymer nanofibers by dissolving the polymer precursors in solvent in 1934.^[17] Besides the original polymeric materials, electrospun materials now also include metals, ceramics, semiconductors and proteins, and combinations thereof.^[13a] Due to the large specific surface area, high porosity, and unique nanostructural and composite characteristics,^[18] electrospun nanofibers encompass great application potential in energy storage,^[19] drug release,^[20] biosensing,^[21] and filtration.^[22] Nowadays, the electrospinning technology is not only limited to research in the laboratory but has also been applied to realistic industrial productions, demonstrating its general scalability.^[23]

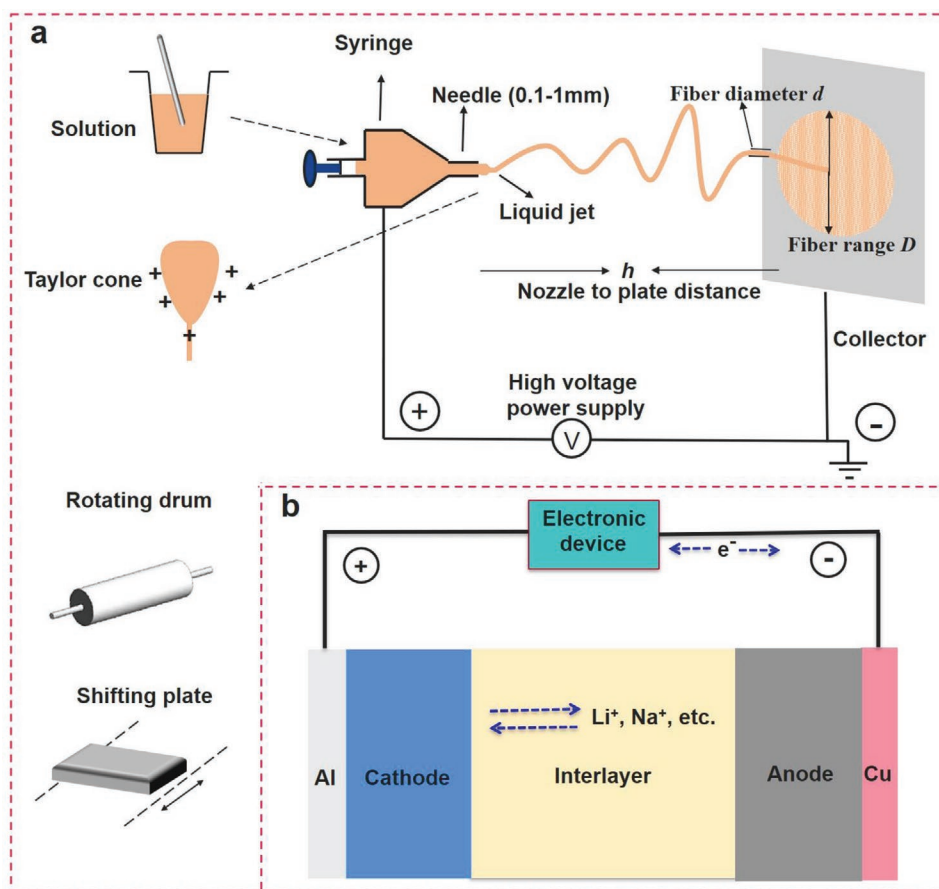


Figure 1. a) Basic illustration of electrospinning setup: nozzle to plate distance h (about 20 cm), fiber diameter d (few to 10^3 nm), fiber range D (similar magnitude as h), needle nozzle inner diameter (0.1–1.0 mm), and applied voltage (1–100 kV). The collector can be a flat plate or drum that can shift or rotate. b) Schematic configuration of alkali-metal ion based batteries with cathode (alkali-metal ion containing oxide, sulfur, etc.), anode (Li, graphite, alloy, etc.), and interlayer (liquid electrolyte and separator, or solid-state electrolyte).

2.1. A Brief History of Electrospinning

Electrostatic atomization was developed in the mid-18th century by Bose,^[24] which has similar physics as electrospinning in that an applied electrostatic field competes against surface tension to increase the surface area of a liquid body. The main difference between electrospinning and electrostatic atomization is that electrospinning is the utilization of high-viscosity (or viscoelastic) fluids. The beginning of electrospinning was widely recognized when Formhals^[17] successfully fabricated textile yarns from cellulose acetate using electrostatic forces and applied for a patent for the device in 1934. In the next decades, a number of papers and patents had been published in the field of electrospinning, which focused on the procedure of preparing continuous, composite, fine fibers and the process of influencing the fiber length.

Initially, the electrospinning theory experienced a rather slow developing period. In 1964, Taylor^[25] proposed the concept of the Taylor cone, a mathematical model for the shape of the fluid droplet formed due to electrostatic forces. Taylor derived the voltage balance equation of the Taylor cone and calculated that the angle of the stable Taylor cone was 49.3° , which was experimentally verified in 1969.^[26]

With the development of nanotechnology and the growing demands for nanomaterials, the 21st century has witnessed a rapid and in-depth development of electrospinning. Reneker, Yarín et al.^[27] developed the experimental phenomenology and theory of electrospinning mechanical process by analyzing the bending instability during flight (**Figure 2a**). They observed the jet path with a high-speed camera and studied the initiation and growth of the bending, whipping and stretching motions that reduce the liquid cross-sectional area by up to $10^5 \times$. Fundamentally, this bending instability and corresponding increase in liquid area are driven by the Coulombic interaction between the same-signed surface charges of the electrically conductive liquid body, which counteracts the surface tension and also the viscoelastic resistance to stretching. Through combined experimental and modeling analyses they found that the typical path of the jet was a straight segment followed by coils with increasing diameters within a larger conical envelope. The bending instability began with the lateral perturbation and the jet then grew into a spiraling coil with an expanding diameter of the coil caused by the repulsive forces between the charged neighboring elements of the jet. A new set of bending instability could appear on the curved coil, featured as a smaller set of spirals looping around the first-coil path. It repeated in a similar pattern of coils until

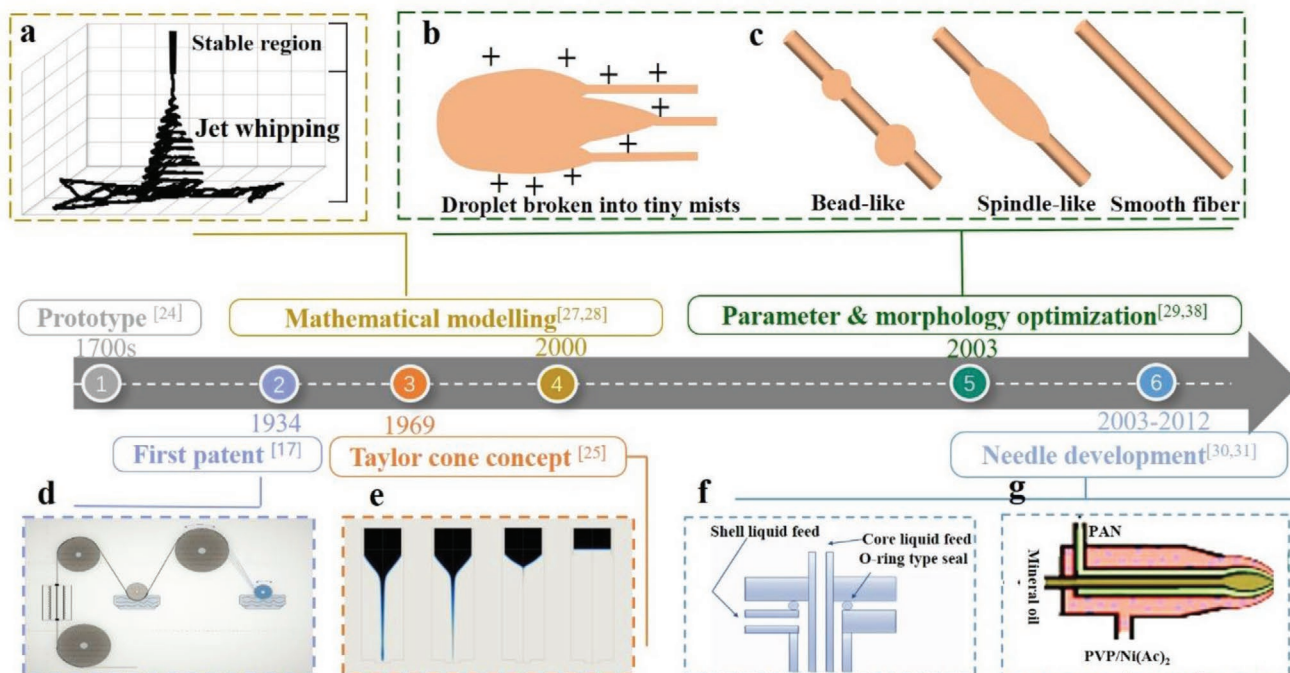


Figure 2. Schematic of the development history of the electrospinning technique.

the solvent evaporated and the solidified polymer resisted further elongation. Finally, thin nanofibers could be gathered on the collector. Rutledge, Brenner et al.^[28] evaluated the effect of processing parameters (electric field, electric current, solution properties, etc.) on fiber diameter and proposed a mathematical model of jet profile and range.^[28] Since these theoretical developments, researches on various process parameters that influenced the fiber have become popular and many schemes have been proposed to optimize the process parameters based on exploratory results. Fridrikh et al.^[29] analyzed dependencies on surface tension, flow rate, and electrical current that determined the diameter of the fluid jet during electrospinning, and then developed a simple analytical model to predict the existence of a terminal jet diameter. In 2003, Larsen et al.^[30] proposed the feasibility of preparing core-shell composite ultrafine fibers by coaxial electrospinning. In 2014, Chen et al.^[31] reported the first triple-coaxial electrospinning technique to synthesize amorphous carbon nanotubules. The electrospinning theory and practice thus experienced comprehensive growth.^[32] Today, the number of research papers on electrospinning for producing functionalized composite nanofibers is still increasing.

2.2. Factors Influencing the Fiber Formation

2.2.1. Electrical Conductivity

The polymer solution must be conductive either by mobile cations/anions and/or free electrons to induce surface charge, like those on the metal plate of capacitors. Indeed, the whipping instability can be regarded as an attempt by the flexible liquid body to morph into a high-capacitance electrode. If the conductivity is low, the charging of such ever-increasing surface area

and capacitance will be sluggish and the electrostatic force may not be able to continue to overcome surface tension and viscoelastic resistance to keep stretching the liquid body (by up to $10^5 \times$).^[33] Selecting a highly conductive solvent (acetone, chloroform, ethyl acetate, etc.)^[34] and adding a salt or an electrolyte have been proven to promote uniform electrospun fibers by suppressing bead formation and reducing fiber diameters.^[35] However, with an excessive electrical conductivity, it can also lead to increasing velocity and solution quantity ejected from the needle. The solvent cannot be completely evaporated before hitting the plate, thus forming bead-like nonuniformities on the fiber (Figure 3).^[36]

2.2.2. Surface Tension

Surface tension is another key factor to ensure continuous electrospinning. Surface tension tends to hinder the jet from becoming longer and thinner, and it has a complicated correlation with other material parameters like viscosity when the liquid solution formulation is tuned. It was reported that by reducing the surface tension of the solution, bead-less fibers could be achieved, since the solvent molecules could spread over the entangled polymer molecules more easily.^[37] Selecting a low-surface-tension solvent or adding a proper surfactant can promote the continuous electrospinning capability.^[38]

2.2.3. Viscoelasticity

The liquid solution is generally quite viscous and can have non-Newtonian flow behavior. Viscosity is one of the most important factors that can determine the length and continuity of electrospun

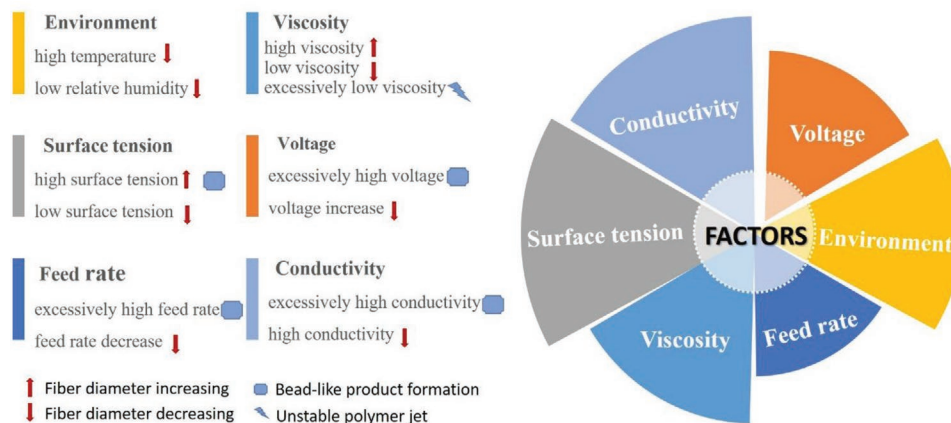


Figure 3. Factors influencing the fiber formation by the electrospinning technique.

fibers.^[39] With a low-viscosity liquid solution, the entanglement between polymer chains is weakened and the resistance of the jet to stretching will be reduced; so the electrostatic force will dominate. With low-viscosity solution, charged droplets will be broken into many tiny mists (Figure 2b) like in electrostatic atomization. Then, with increasing viscosity, the mist particles will connect up and the shape of beads in the fiber will transform from spherical to spindle-like until a smooth fiber forms (Figure 2c). At an even higher viscosity, the charged jet is unable to undergo sufficient stretching and refining, yielding larger fiber diameters with a wider fiber diameter distribution.^[38] In 2005, the scaling relationship between viscosity and fiber diameter was studied, that is, $d_f = k_2 \eta^n$, where η and d_f represent viscosity and fiber diameter, respectively, k_2 is a constant and n depends on polymer precursor.^[40] Generally, viscosity is related to polymer molecular weight and its concentration. Increases of molecular weight and concentration hence enable higher polymer entanglement and larger viscoelasticity and non-Newtonian behavior.

2.2.4. Voltage

The voltage value will directly influence the electric field intensity and thus the electric forces on the Taylor cone and jet.^[41a] Below a certain threshold, when the voltage is increased, more ejection of polymer solution and smaller-diameter uniform nanofibers can be obtained. However, when surpassing the threshold value, further increase of the voltage will make the process more unstable and more beads will appear on the fiber, similar to the water beads-on-fiber situation of spider web at dawn.^[41b]

2.2.5. Feed Rate

Feed rate is another processing factor that greatly affects the diameter and geometry of the fiber formed. When the feed rate is too high from the pressurized spinneret, too much solution is ejected, and hence the tensile stress acting on the polymer relatively decreases and forms nonuniform fiber or beads. However, when the feed rate is too low, needle blocking issues will arise because of evaporation of the solvent.^[26]

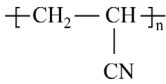
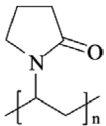
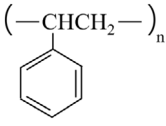
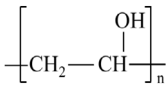
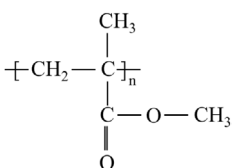
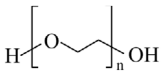
2.2.6. Environment

Environment is another critical factor that affects the solidifying process by influencing the solvent evaporation.^[42] First, the solidifying process can take place either in air or in an inert gas, which mainly affects how quickly solvent will be evaporated in flight. Second, two other parameters of temperature and humidity should also be considered. High surrounding temperature causes high solvent evaporation rate and the charged jet will take a shorter time to solidify. Humidity mainly affects the dissipation rate of the stored charges on the polymer jet during electrospinning. When the humidity is high, the surface charge on the jet leaks quickly (akin to a leaky capacitor) and the stretching effect is weak, thus producing spun fibers with larger diameters. Besides, small pores on fiber surface can be formed by increasing the humidity because of the evaporative cooling and water condensation processes during solidification.^[43] However, if the humidity is too low, the solvent on the needle tip will evaporate too quickly, resulting in clogging of the needle tip.

2.2.7. Polymer

Polymer type and concentration are important factors for fiber formation.^[35,44] Various polymers present different physical and chemical properties, and can be dissolved in different solvents (Table 1). When polymers are dissolved to make the electrospinning solution, polymer chain entanglement will form in the solution, which determines the solution viscosity. Higher molecular weight of the polymer leads to higher chain entanglement that is beneficial for electrospinning. This is because a higher viscosity can help elongate the polymer solution to form fibers.^[35,45] But it may also affect the solubility of the polymer in the solvent. Generally, different polymers show different chain entanglements in the electrospinning solutions, which affect the diameters of the formed fibers (Table 1). For example, polyacrylonitrile (PAN) is usually dissolved in dimethyl formamide (DMF) to obtain the electrospinning solution. After electrospinning, PAN nanofibers can be produced with diameters ≈ 100 nm.^[44c] However, for polystyrene (PS) solution with the same concentration, the formed PS nanofibers show much larger diameters (≈ 600 nm) when compared to those of PAN.^[35]

Table 1. Properties of some typical polymers and their corresponding electrospun fiber diameters.

Polymer	Structural formula	Electrospinning solution (polymer/solvent) Molecule weight, concentration	Melting point [°C]	Fiber diameter [nm]	Ref.
PAN		PAN/DMF $M_w = 100\,000$, ≈ 10 wt%	317	≈ 100	[44c]
PVP		PVP/Ethanol $M_w = 1\,300\,000$, ≈ 10 wt%	130	≈ 1500	[44b]
PS		PS/DMF $M_w = 280\,000$, ≈ 10 wt%	240	≈ 600	[35]
PVA		PVA/water $M_w = 78\,672$, ≈ 10 wt%	230–240	200–500	[44a]
PMMA		PMMA/DMF $M_w = 60\,000$, ≈ 8 wt%	130–140	≈ 300	[44d]
PEO		PEO/water $M_w = 300\,000$, ≈ 6 wt%	62–64	≈ 300	[44e]

2.3. The Combined Synthetic Technique

By the end of the 20th century, the electrospinning technique has made significant advances both in theoretical developments and processing approaches. With the fast developments of nanotechnology in recent years, electrospinning associated with other technologies (e.g., sol-gel, hydrothermal method, chemical vapor deposition (CVD), etc.) has received extensive attention because together they enable an extremely powerful synthetic strategy that can be used to tailor the structural and compositional features of porous nanomaterials (Figure 4). Various composite nanomaterials with diverse hierarchical architectures have been reported, for example, electrospinning associated with CVD. There are different kinds of CVD, such as low-pressure CVD, plasma-enhanced CVD, and high-vacuum CVD.^[46] The CVD techniques are frequently used to prepare energy storage materials, such as carbon nanotubes (CNTs), graphene, carbon balls, carbon nanofibers (CNFs), and Si nanowires.^[47] If the CVD method is collaboratively introduced into the prepared electrospun nanomatrix or nanoframework, we can achieve advanced materials with hierarchical porous structures.^[47e] In 2004, Hou and Reneker proposed a novel electrospinning and CVD process to obtain hierarchical nanostructures.^[47a] They introduced an iron compound into PAN nanofibers, followed by calcination to obtain iron particles on CNFs. The Fe nanoparticles on CNFs would catalyze the growth of CNTs when using hexane as a carbon source

to form CNT/CNF hybrids. For such hybrid architectures, the CNTs grown by CVD could help increase electron conductivity,

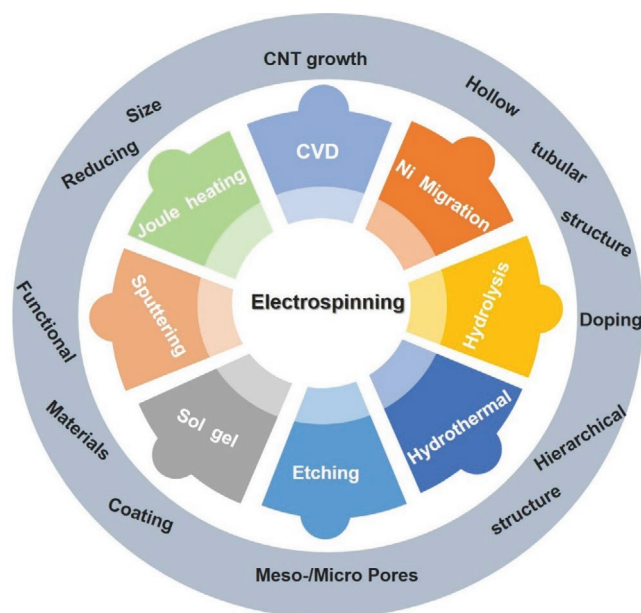


Figure 4. Overall schematic showing combinations of the electrospinning technique with other materials processing approaches to enable different hierarchical structures and diverse nanomaterial hybrids.

while the electrospun CNF network provides the structural stability of the matrix. Other active materials can further grow onto such architectures to form novel composite hierarchical structures. For example, Liang et al.^[47h] further applied a vaporization–condensation fumigation method to anchor red phosphorus (P) onto CNT/CNF hybrids. The prepared dual-network architecture possessed large surface areas and high porosity, which could accommodate the large volume change and enable high Li⁺ ion diffusivity upon charging/discharging. As a result, the prepared P@CNT/CNF composite showed good rate capability (600 mAh g⁻¹ at 3 A g⁻¹) and long cycling life up to 500 cycles. In addition, the CVD method can also be used to grow other active materials, such as Si, onto the prepared electrospun nanosubstrates. For example, Cui et al. used CVD to grow a thin Si layer (30 nm) with the SiH₄ precursor onto the prepared electrospun CNFs to form core–shell carbon/Si composite nanofibers.^[47b] To further introduce a hollow structure into the hybrids, a simple calcination was employed to remove the carbon in the core, while it also partly oxidized Si to form double-wall Si–SiO_x composite nanotubes. The SiO_x in outer shell and the inner porous structure could help maintain the integrity during cycling and enabled a stable SEI. As the anode for LIBs, the double-wall composite displayed long cycling life for over 900 cycles.

Beside CVD, electrospinning-based strategies also include many other associated synthetic approaches. For example, the sol-gel technique was reported to collaborate with electrospinning method to obtain 1D porous TiO₂ nanofibers^[48] which exhibited higher photocatalytic activities. Also, electrospinning associated with hydrothermal method was reported to achieve the novel hierarchical nanostructures constructed from ZnO branches and TiO₂ nanofibers.^[49] In addition, Zhou et al. incorporated sputtering with electrospinning technique^[50] to deposit a layer of SiC on electrospun polyvinylpyrrolidone (PVP) nanofibers to form core–shell PVP@SiC nanofibers. Through calcination in air for the removal of PVP core, SiC nanotubes were prepared.

Clearly, electrospinning has become a basic technique that closely integrates with other approaches to fabricate advanced nanohybrids with unique structural and compositional advantages for energy storage applications. It usually provides a large-area ($D \approx 10$ cm) structural framework, with potential electrical percolation, as the substrate, and prepositioned chemical precursors for later growth, reactions, or etching. Naturally, the degree of chemical, electrical, photonic, magnetic, and electrochemical functionalization is almost infinite.

3. Examples for Battery Applications

3.1. Building a Carbon Tubular Network for the Electrodes

3.1.1. Electrospinning + Ni⁰ Nanoparticle Migration

Amorphous CNFs could be obtained by carbonization of the prepared electrospun polymer nanofibers (e.g., PAN).^[10c] However, further graphitization of the amorphous CNFs to enhance the electronic conductivity of the electrode is often highly desirable. One way for increasing the degree of graphitization is to use

metallic catalysts such as Ni, Co, Fe, etc., in a reducing atmosphere. Stationary catalysts, however, still suffer from certain limitations. The catalyst particle has a capability to graphitize only ≈ 5 nm thick carbon.^[31a] Thus, carbons in distance beyond the catalytic range (≈ 5 nm) from stationary catalyst particles will still remain amorphous. A better graphitization method is required, for example, a mobile metal nanocatalyst that extends and contracts like a worm, aka peristaltic locomotion.^[31b,c] If a shell is broken from inside, a new worm emerges. As the worm moves, it creates a hollow tunnel structure. Inspired by this, we explored a novel method with which we could take advantage of the migrations of the catalyst nanoparticle (Ni⁰) to graphitize more amorphous carbons and create more hollow tunnels (Figure 5a).^[14a] The Ni⁰ particle was initially encapsulated in CNFs. By changing the heating condition, the Ni⁰ particle would migrate out of the catalyzed graphitic layer into the amorphous carbon region. Once the Ni⁰ particle contacted the amorphous carbons, it elongated: the Ni⁰ morphology changed from a nanosphere into a wormlike shape. Such morphological changes could increase the contact surface area with Ni⁰ and thus increase the graphitic carbon regions. Finally, the wormlike Ni contracted to its original nanospherical shape. This process produced interconnected graphitic hollow tubule (GHT) networks inside CNFs with an inner diameter of ≈ 10 nm and graphitic wall thickness of ≈ 5 nm. Clearly, using Ni⁰ migration is an efficient approach to in situ build up graphitic hollow tunnel networks inside electrospun CNFs so as to enhance their electronic conductivity and certain type of porosity.

Moreover, we can also graft genuine CNTs onto electrospun CNFs to further enhance their conductivities. The CVD method can enable the growth of CNTs onto CNFs, catalyzed by Ni particles and using C₂H₂ gas as a carbon source. We introduced a novel way to grow CNTs onto electrospun CNFs by Ni⁰ migration (Figure 5b).^[51] We found that polymethyl methacrylate (PMMA) could decompose to produce pores and form some C₂H₂ in inert gas at 700 °C. So, we added PMMA and Ni(Ac)₂ into the PAN solution to form a mixture that could be transformed to PMMA/Ni(Ac)₂/PAN composite nanofibers by electrospinning. During the heat treatment in H₂/N₂, PAN and Ni(Ac)₂ were converted to amorphous carbon and Ni particle, respectively, while the decomposition of PMMA produced some C₂H₂. The CNTs grew with the produced C₂H₂ gas, accompanying the Ni⁰ particles migrating from the surface of electrospun CNFs to the tip of the formed CNTs. Therefore, CNT networks were in situ formed onto the electrospun CNFs, producing the CNT/CNF hybrid. When used as an anode for LIBs, this composite anode showed high capacity and good rate capability.

As shown above, Ni⁰ nanoparticle migration not only can produce graphitic hollow tunnel structures inside amorphous CNFs, but also graft genuine CNT networks onto the CNFs, to enhance the conductivity. Other classic studies have also confirmed the above findings for the Ni⁰ migration method workable for other carbon materials.^[47e,52] For example, with methane as carbon source, Helveg et al.^[52b] found that during the growth of CNTs, the nucleation/growth of the graphene layer was aided by the dynamic formation/restructuring of monoatomic step edges at the Ni surface. The reshaping of Ni nanoparticles helped to align graphene layers into a hollow tubular structure. The elongation/contraction processes repeated, leading to the growth of CNTs.

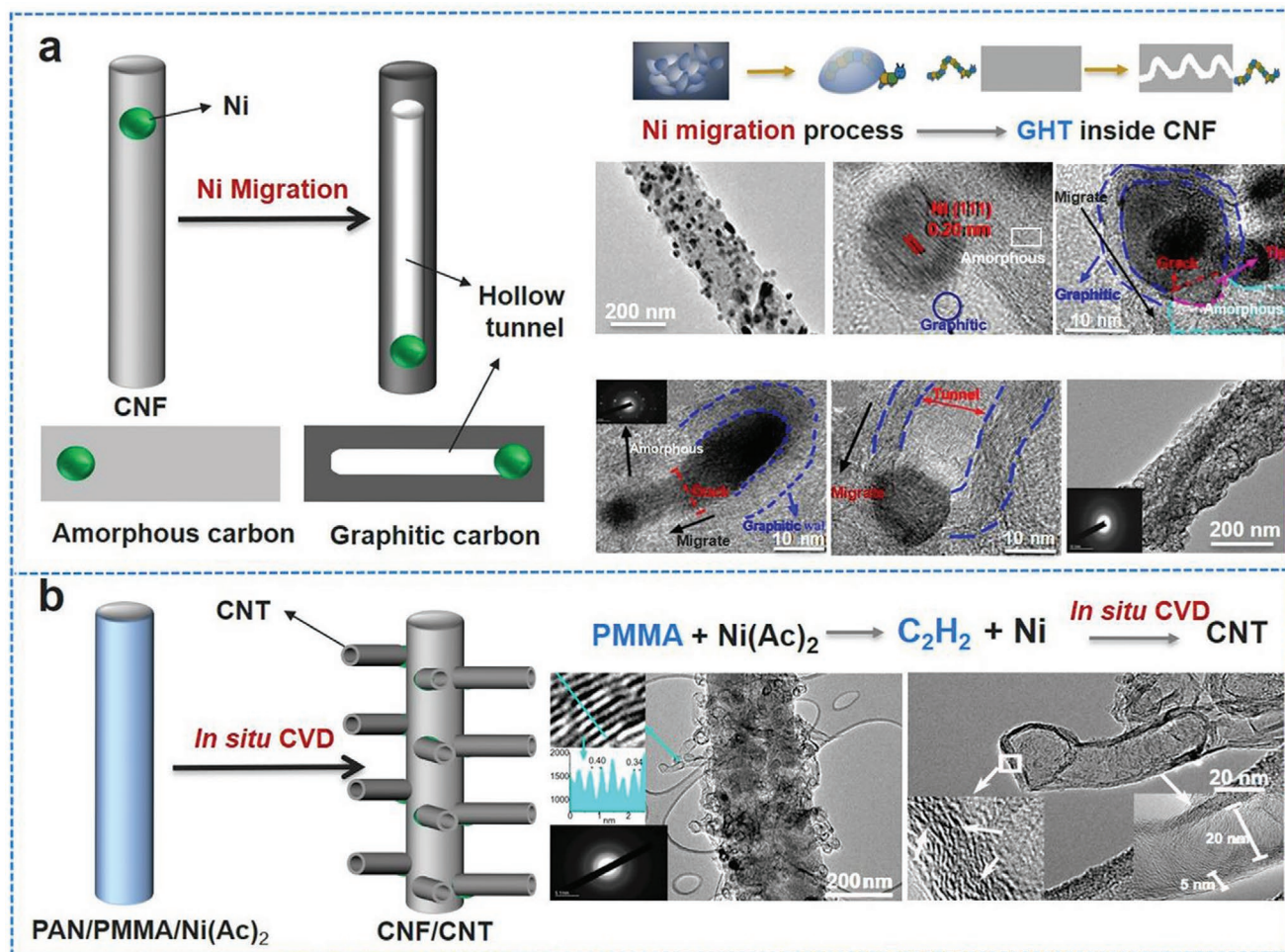


Figure 5. a) Creating a carbon hollow tubule (CHT) structure inside CNFs by a combined Ni⁰ nanoparticle migration and electrospinning process. Adapted with permission.^[14a] Copyright 2014, Royal Society of Chemistry. b) Growth of CNTs onto CNFs by an integrated electrospinning and in situ CVD process. Adapted with permission.^[51] Copyright 2013, American Chemical Society.

The modeling showed that the growth mechanism involved the surface migration of carbon and Ni atoms. For another example, Anton^[52a] found that upon heating a Ni⁰ particle on a thin film of amorphous carbon, the particle was initially encapsulated by a graphitic shell, and then was expelled and migrated on the substrate to graphitize more amorphous carbons.

3.1.2. Electrospun Polymeric Template + Hydrothermal Method

Anode candidates such as metal oxides and metal sulfides have attracted much attention because of their high theoretical capacities. But these high-capacity anode materials show poor conductivity and large volume change during cycling.^[53] A strategy of combining the electrospun polymeric template with the hydrothermal method is a promising solution. Specifically, the high-capacity metal oxide and metal sulfide materials can be synthesized by the hydrothermal method, which can be attached to a carbonaceous network to enable fast electron transport. Also, a hollow structure can be created by removal of the electrospun polymer template to accommodate the large

volume change of these anodes during cycling. The above architectures, enabled by electrospinning, can allow fast ionic and electronic transport while maintaining the stable structure of the metal-based anodes. An example with such strategy was proposed by Chen et al. (Figure 6a).^[14b] They added some functional CNTs into the PAN solution. During the electrospinning process, CNTs were aligned along the streamline of the electrospinning solution due to the elongation and surface tension of the fluid jet, forming the tube-in-fiber CNT/PAN composite fiber template. A protective layer of CoS was grown onto the composite fiber template to maintain the integrity during the following hydrothermal process. When further combined with a simple hydrothermal method, two interesting results could be achieved: i) a layer of MoS₂ formed onto the surface of the protective layer of CoS on the CNT/PAN composite fiber and ii) PAN was removed to create a hollow tunnel structure. After a further combined heating treatment and acid process, the tube-in-tube structure was produced (Figure 6a), with the CNT (core) aligned with the metal sulfide nanotube (shell) that was constructed from 2D atomic sheets of MoS₂ with only 2–5 layers. Finally, the thickness of the metal sulfide shell could be further

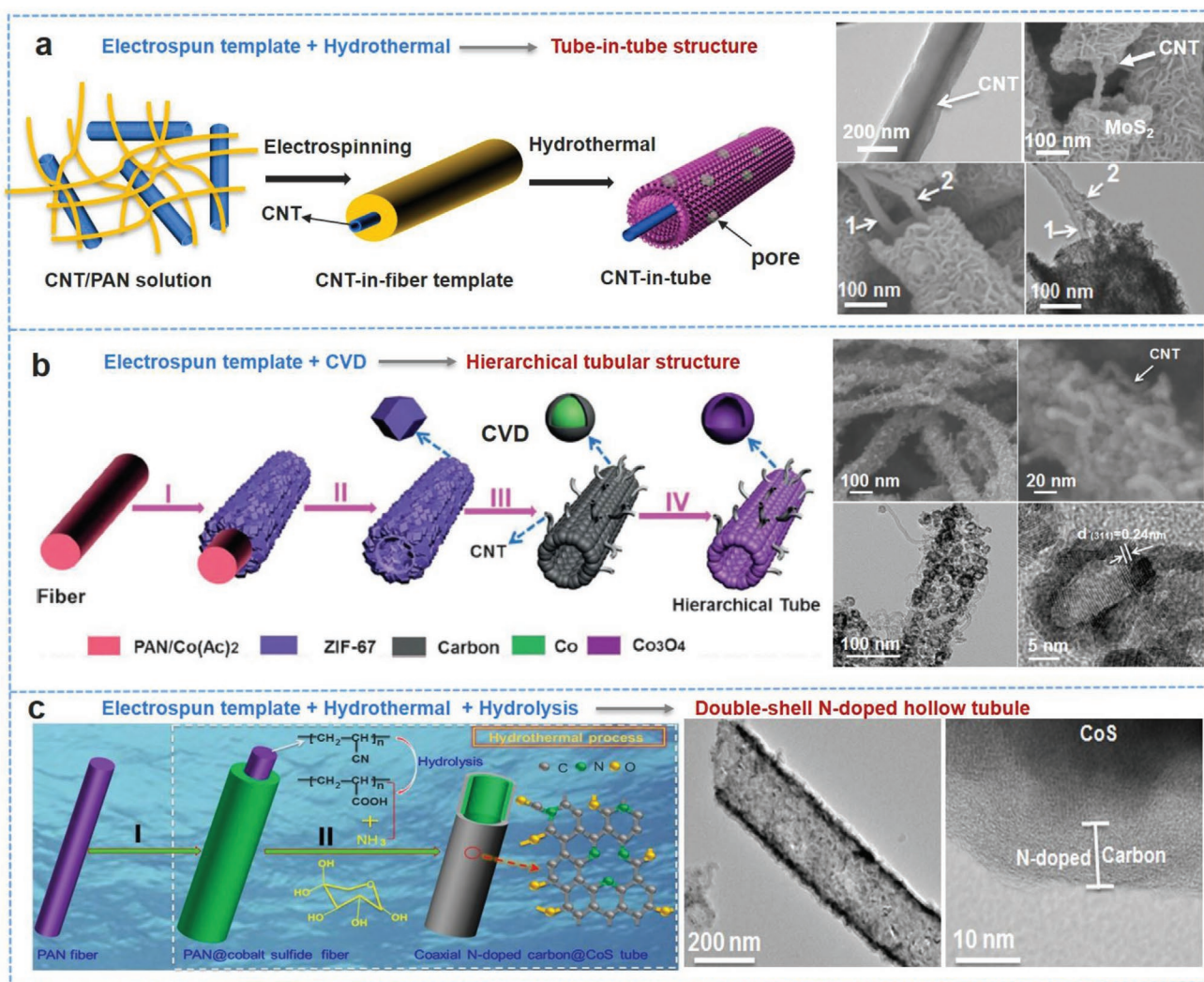


Figure 6. Combining electrospun polymeric template with: (a) hydrothermal method for the formation of tube-in-tube structure. Adapted with permission.^[14b] Copyright 2016, AAAA, (b) CVD technique for synthesis of the hierarchical tubular structure. Adapted with permission.^[54] Copyright 2016, Wiley-VCH, and (c) hydrothermal and hydrolysis for the preparation of double-shell N-doped carbon/CoS_x hollow tubules. Adapted with permission.^[55] Copyright 2016, Wiley-VCH.

tuned from 50 to over 100 nm by adjusting the corresponding precursor. The types and number (from 1 to 4) of CNTs inside the metal sulfide nanotubes could also be controlled. When used as an anode for LIBs, this tube-in-tube hybrid manifested high capacity of $\approx 1300 \text{ mAh g}^{-1}$, excellent rate capability and long cycling life for over 1000 cycles. After cycling, the tube-in-tube structure was still maintained, thus indicating the advantage of such a hierarchical structure.

3.1.3. Electrospun Polymeric Template + CVD

We have introduced growing CNTs by CVD onto electrospun CNFs to enhance the electronic conductivity. Electrospinning associated with the CVD process can also achieve more complex structures for the CNT/metal-based anode hollow composite. Generally, to achieve this goal, electrospun fibers can first be produced as the template. Second, a functional layer can be

grown onto the electrospun fibers, which would later be converted into the composite of CNT/metal-based anode, whereby the CNT growth is facilitated by the CVD process. The key point for this strategy is to find a proper component for the outer functional layer. Among many materials, zeolitic imidazolate framework-67 (ZIF-67) is a typical selection, which can be converted to CNTs and Co nanoparticles during the CVD process, and then Co can be easily converted to Co₃O₄ upon heating in air. For example, Chen et al.^[54] introduced the component of cobalt acetate into electrospun polymer nanofibers to serve as a typical source for the growth of ZIF-67 (Figure 6b). The cobalt ions in the polymer nanofibers could react with 1,2-Dimethylimidazole, and thus forming a surface layer of ZIF-67. The core of the composite fibers could be removed by organic solvent to form ZIF-67 hollow tubules. A simple two-step heating treatment was then applied. For the first step, the ZIF-67 hollow tubules were heated in H₂/N₂ gas to form the Co/carbon composite, while Co acted as a catalyst to facilitate the in situ growth

of CNTs on Co/carbon hollow tubules (CVD process). For the second step, a relatively low-temperature calcination treatment (350–370 °C) in air was chosen to not only oxidize Co to Co₃O₄ accompanied by the morphological evolution from particles to hollow nanospheres due to the Kirkendall effect, but also burn out these carbons in the composite tubules, leading to the formation of the hierarchical tubular structures composed of hollow Co₃O₄ nanospheres and CNTs. When used as the anode for LIBs, the hierarchical tubular architecture manifested a high capacity of 782 mAh g⁻¹ after 200 cycles at 1 A g⁻¹.

3.1.4. Electrospun Polymeric Template + CVD + Hydrothermal Method

As mentioned in the above paragraph, through a combined electrospinning and CVD method, it could reach the hierarchical architectures of CNTs on Co/carbon hollow tubules. The Co particles were nonactive materials and could not serve as the anode for LIBs. As a solution, a simple hydrothermal process could be further added to sulfurize Co in the carbon to form CoS_x, which is a promising anode with high capacity. The tests on LIBs with the obtained ultrafine CoS_x nanoparticles in hierarchical carbon tubules also showed superior lithium storage properties of 592 mAh g⁻¹ at 5 A g⁻¹ after 1600 cycles.^[10e]

3.1.5. Electrospun Polymeric Template + Hydrothermal Method + Hydrolysis

Usually, the process to achieve the hierarchical tubular architecture is as follows: first, the electrospun polymeric template is dissolved in organic solvent to create hollow structures; then using the above hollow structures as the substrate, the hydrothermal method is employed to synthesize the proposed materials onto them and then form the hierarchical tubular structures. This combined process is complex and consumes organic solvent. A better idea is that these two steps can be merged into one, i.e., during the hydrothermal step, the polymeric template could also be removed. There are two ways to achieve this. One is to select typical polymers that can decompose during the hydrothermal process. The other is to convert the polymers that are not dissolvable in solvent (e.g., water) to polymers dissolvable in solvent during the hydrothermal process. In 2016, with Goodenough, we exploited such a novel method to enable the hydrolysis of polymer induced by a simple hydrothermal process (Figure 6c).^[55] First, a layer of cobalt sulfide (CoS_x) was loaded onto the surface of the PAN nanofibers by a solvent process. Then, a simple glucose-based hydrothermal step was designed, from which it was found that the CN group within PAN went through the hydrolysis process and was transformed into COOH. This process converted the aqueous-undissolvable PAN core into aqueous-dissolvable hydrosoluble polyacrylic acid (PAA), and thus produced the hollow tubular structures of CoS_x. The related reaction was $\text{CN} + 2\text{H}_2\text{O} \rightarrow \text{COOH} + \text{NH}_3$. Interestingly, NH₃ formed from the hydrolysis would also involve in the carbonization of glucose and form N-doped carbon onto the surface of CoS_x nanotubes, which enables the double-shell N-doped carbon/CoS_x hollow

tubules structure. The hollow tubular hybrid showed high reversible capacity of ≈506 mAh g⁻¹ at 1.25 A g⁻¹, with a good rate capability (569, 475, and 396 mAh g⁻¹ at 1, 2, and 3 A g⁻¹, respectively), when evaluated as an anode for sodium-ion batteries. Meanwhile, the carbon@CoS_x tubules also displayed exceptional cycling performance over 1400 cycles at 3 A g⁻¹.

3.1.6. Electrospinning + Carbothermal Reduction Etching

Here, we introduce another electrospinning-based strategy associated with the carbothermal reduction etching process, which enables a variety of nanocarbons with different and controllable porosities from porous CNFs to porous carbon hollow tubules (CHTs). This novel electrospinning-based method was developed by Chen et al. (Figure 7) by associating with the carbothermal reduction to perform a self-etching process.^[56] First, mixed Zn(Ac)₂ and Co(Ac)₂ were introduced in PAN nanofibers to provide metal ions for in situ growth of a bimetallic metal–organic framework (MOF) layer on the composite nanofibers. This would yield PAN/metal salt@bimetallic MOF core–shell nanofibers. In heat treatment, the core and shell contributed to different roles. The bimetallic MOF shell would form the N-doped porous carbon shell with a high degree of graphitization. Different from the shell, during the heating process, the core experienced initially a conversion reaction that PAN and metal ions transformed into carbon and ZnO, and then the etching of carbon by ZnO based on the carbothermal reduction of $\text{ZnO} + \text{C} \rightarrow \text{Zn} + \text{CO}$ or CO_2 . Through control of the amount of Zn(Ac)₂, the content of ZnO was well modulated to etch part or all of the carbon, enabling either a porous carbon core or a hollow tubular structure. Thus, a variety of nanocarbons from porous CNFs to porous CHTs could be obtained.

Furthermore, such a self-etching method was also extended to synthesize other CHT-based hybrids. For example, besides metal cations, graphene nanosheets were also added into the PAN solution. Following a similar process, graphene nanosheets were sandwiched between CHTs, forming the porous CHT/graphene composites. This approach could well control the various factors that influence the electrochemical performance of carbons, including multilevel hierarchical pores, graphitization degree, and large enough interlayer spacing. Owing to these combined advantages, the synthesized porous CHTs showed high electrochemical performance with a high capacity of 346 mAh g⁻¹ and an ultralong cycling life over 10 000 cycles without clear fading of capacity, when used as an anode for sodium-ion batteries. The superior performance of the prepared CHTs can be ascribed to the following features: i) many defects and pores that serve as reservoirs to store Na ions,^[11b] ii) high surface area to provide short diffusion distance for Na⁺, and iii) 1D structure and high graphitization degree.^[57]

3.2. Developing 3D Nanoframeworks as Li Metal/Sulfur Hosts

3.2.1. As a Sulfur Host

Li–S battery is a promising alternative to LIBs because sulfur can deliver a high theoretical capacity of 1675 mAh g⁻¹ with an

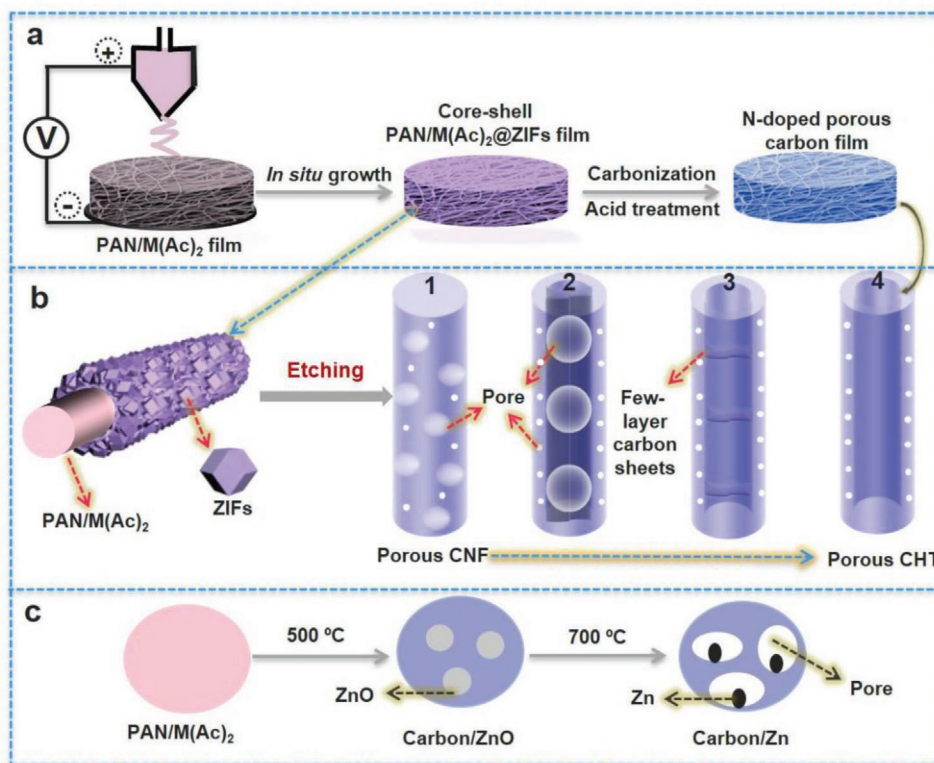


Figure 7. Combining electrospun template with etching for synthesis of a range of nanocarbons from porous CNFs to carbon hollow tubules, where ZnO from the conversion of $\text{Zn}(\text{Ac})_2$ etched the carbon based on the carbothermal reduction: $\text{ZnO} + \text{C} \rightarrow \text{Zn} + \text{CO}$ or CO_2 . Through control of the amount of $\text{Zn}(\text{Ac})_2$, the content of ZnO could be well modulated to etch part or all of the carbon, enabling either a porous carbon core or a hollow tubular structure. Adapted with permission.^[56] Copyright 2017, Elsevier.

exceptional theoretical energy density of 2567 Wh kg^{-1} .^[58] Moreover, sulfur is low cost and environmentally benign.^[59] However, several challenges hinder their applications including the poor electrical conductivity of sulfur and Li_2S , high solubility of polysulfide and large volume change of 80%,^[4c] which lead to low rate capacity, poor Coulomb efficiency, and fast capacity degradation.^[60] Due to the high electrical conductivity, porous structure, and excellent mechanical stability, porous carbon nanomaterials are widely chosen as sulfur hosts, which can enable fast electron transport, effective ion diffusion, good accommodation of volume change, and absorption of polysulfide. The electrospinning-based technique has become research hotspot on the preparation of CNFs with different porous structures from 0D hollow spheres to 1D hollow channels.^[61] Among various polymers, PAN is the primary precursor to prepare carbon materials; while the organic or inorganic templates, such as sacrificial polymer, metal oxide and metal, are widely used to create pores in the carbon matrix. For the preparation of 0D hollow spheres inside electrospun carbons, the selected template should have a spherical morphology. Templates with a spherical morphology inside the electrospun fibers can either be added directly into the electrospinning solution followed by electrospinning or formed in situ from their precursors inside the electrospun fibers during calcination. For example, Ni nanospheres were in situ formed inside the electrospun CNFs by the decomposition of $\text{Ni}(\text{Ac})_2$ in PAN nanofibers. By a simple acid treatment, Ni^0 nanospheres were removed to create hollow

nanospheres inside porous CNFs. Also, another way is to add the SiO_2 nanospheres as the template into the PAN solution. During the electrospinning process, the SiO_2 nanospheres were integrated inside the PAN nanofibers. After a combined heating and etching process, PAN on SiO_2 nanospheres was converted into carbon, while the SiO_2 nanospheres were removed, thereby yielding hollow-carbon-sphere (HCS)-integrated nanofibers. When working as the sulfur host, these 1D nanocarbons with hollow spheres provided space to store sulfur and also accommodated its large volume change. The final prepared carbon (C)/S composite achieved good electrochemical performance.^[62] Lately, a recent study demonstrated that the yolk-shell structure was better than the hollow sphere when used as a sulfur host, since it could take advantage of the features from both the core and shell. Furthermore, the shell inside the hollow sphere enabled a safeguarding interspace to enhance structural integrity during cycling and an inner path for electron and ion diffusion to promote the electrochemical reaction (Figure 8a).^[62] The yolk-shell carbonaceous fiber freestanding cathode could deliver a high capacity after 500 cycles at 1C with only 17.2% fading. Meanwhile, this electrode also showed an exceptionally high areal capacity of 15.5 mAh cm^{-2} .

When compared to hollow nanospheres, a hollow channel inside CNFs shows more advantages due to its 1D structure that is beneficial for electronic and ionic transport. The main method to create hollow channel inside CNFs is to form a 1D template inside electrospun nanofibers. After the removal of

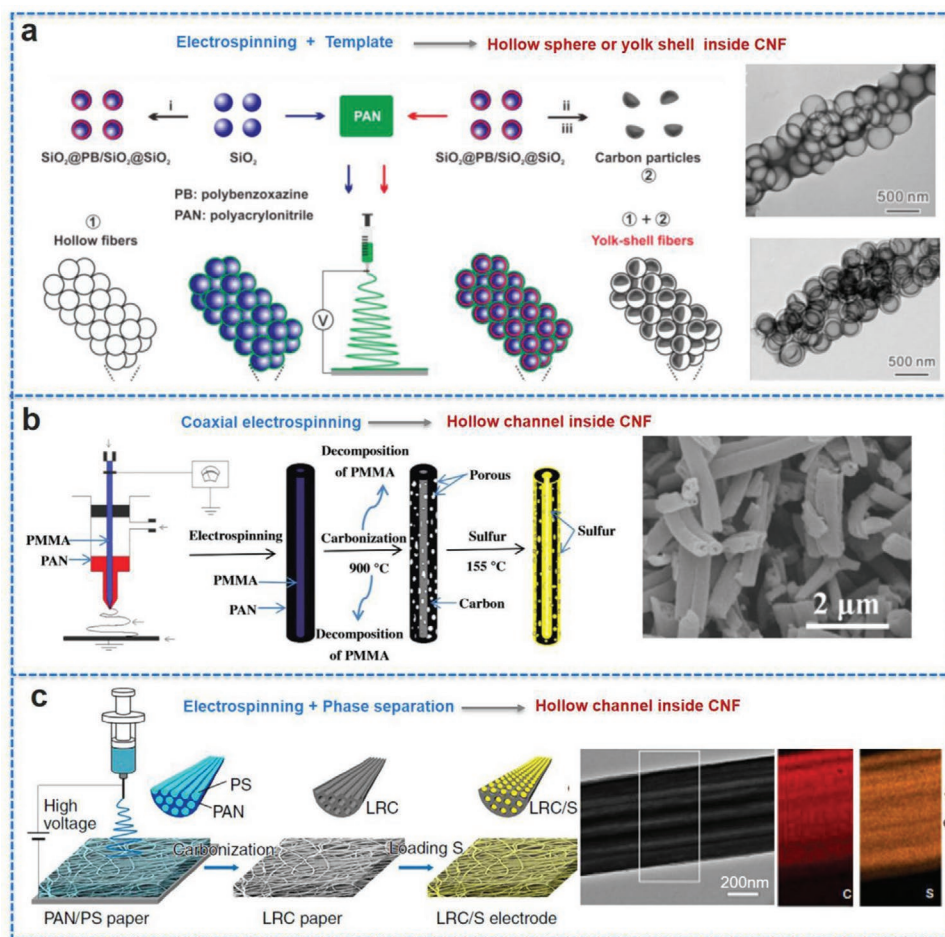


Figure 8. a) Formation of hollow nanospheres and hollow yolk–shell structure inside CNFs as sulfur host by electrospinning technique combined with template. Adapted with permission.^[62] Copyright 2018, Elsevier. b) Coaxial electrospinning technique enables hollow CNFs as sulfur host. Adapted with permission.^[64] Copyright 2014, Elsevier. c) Combined electrospinning technique and phase separation enables hollow channels inside CNFs as sulfur host. Adapted with permission.^[58] Copyright 2015, Springer Nature.

the template, the 1D hollow channel can be created inside the CNFs.^[63] Coaxial electrospinning is an important tool for producing 1D core–shell structures with sacrificial templates as the core, including oil and polymer. These sacrificial templates are used as the inner solution while the carbon source (PAN, etc.) is used for the outer solution. Wu et al. used PMMA and PAN as the inner and outer electrospinning solutions to prepare core–shell PMMA@PAN nanofibers that were carbonized to obtain porous hollow CNFs (Figure 8b).^[64] The prepared porous hollow CNF/S cathode delivered a high capacity up to 815 mAh g⁻¹ at 0.1C. Also, by taking advantage of the separation of polymers, Li et al.^[58] used a simple single-nozzle electrospinning technique to introduce multichannels inside CNFs (Figure 8c). When PAN and PS were added to DMF solvent, PAN became the continual phase while PS was the discontinuous phase. During electrospinning, the solution retained phase separation with the PAN nanofiber encasing the elongated 1D PS multi-nanofibers. After calcination at 800 °C in Ar, many hollow channels were created inside the PAN nanofiber akin to a lotus root-like multichannel carbon (LRC) nanofiber, which can be subsequently loaded with sulfur. These hollow C/S cathodes showed good electrochemical capacity. Besides, Chen et al. introduced both hollow spheres and hollow tubes to

CNFs by a combined electrospinning and CVD process as mentioned earlier.^[61a] Specifically, the hollow nanospheres were created inside CNFs, and CNTs were grown on CNF surface. After impregnating sulfur, the porous hollow CNT/CNF/S showed a high capacity and long cycling life at a high rate.

Doping or mixing with other functional materials such as metal impurity (Ni, Fe, Cu, etc.),^[65] metal oxide/sulfide (TiO₂, La₂O₃, MoS₂, etc.),^[66] and metal carbide/nitride/fluoride (Mo₂C, TiN, CeF₂, etc.)^[67] not only can form strong chemical bonding with sulfur or polysulfide during cycling, but also can promote the redox reaction of active materials. Adding their corresponding precursors into the electrospinning solution is a common method to obtain porous CNFs with doped functional materials. Deng et al. proposed a novel CeF₃-doped hierarchical porous CNFs by carbonizing polyvinyl alcohol (PVA)/polytetrafluoroethylene (PTFE)/boric acid (BA)/CeCl₃ composite nanofibers.^[68] Many pores in the prepared samples would store sulfur to enable high capacity. CeF₃ played a catalytic role in the reduction of sulfur and suppression of migration of polysulfide through physical/chemical interaction, leading to high rate capability and long cycling life. Consequently, the obtained CeF₃-doped C/S showed much improved capacity up to 1395.0 mAh g⁻¹ and better capacity retention of 901.2 mAh g⁻¹ after 500 cycles.

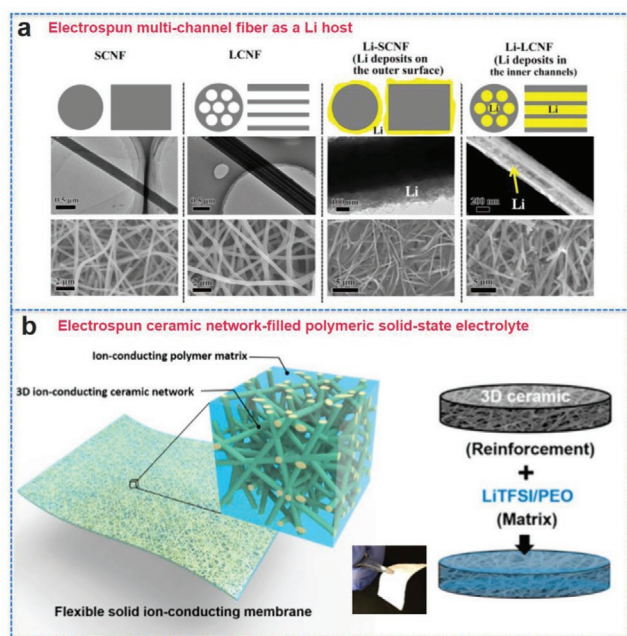


Figure 9. a) Electrospun hollow-channel fiber as a Li metal host. Adapted with permission.^[72] Copyright 2017, Elsevier. b) Electrospun ceramic network as a 3D matrix for polymeric solid-state electrolyte. Adapted with permission.^[78] Copyright 2016, National Academy of Sciences.

Also, post-treatment is another extremely favorable way for the decoration of functional materials onto porous CNFs. For example, a simple hydrothermal method was adopted by Xue et al. to grow ivy-structured MoS_2 nanoflakes on porous N-doped CNFs.^[67b] MoS_2 nanoflakes formed on porous CNFs would show strong chemical binding with polysulfide, hence promoting fast redox reaction kinetics of the sulfur cathode.

3.2.2. As a Li Metal Host

Utilizing Li metal in the body-centered cubic (BCC) crystal structure as the anode is the holy grail with the highest theoretical capacity (3861 mAh g^{-1}) and lowest electrochemical potential (-3.04 V vs NHE).^[69] However, its practical application has been hindered by several issues, including the formation of Li dendrite, large volume change, and instability of the interfaces.^[70] 3D electrospun porous carbons have been widely studied as current collectors for Li_{BCC} anode due to abundant active sites for the decrease of the current density of anode and their sufficient space for Li deposition and accommodation of large volume change during Li_{BCC} plating/stripping.^[71] By a combined electrospinning and template process as mentioned above, these prepared porous CNFs as a sulfur host can also be employed to store Li metal. Xiang et al. demonstrated that a lotus root-like hollow CNFs with proper interior to exterior radius ratio would guide Li^+ to plate on the inner surface of the channels inside the CNFs because of the drifting effect induced by the structural stresses (Figure 9a).^[72] Also, they coated a lithiated Nafion layer onto the hollow CNFs as a solid electrolyte interface to further stabilize the interface of Li metal for a better Coulombic efficiency with a high capacity over $3600 \text{ mAh g}^{-1}_{\text{carbon}}$. However,

the weak affinity of carbon for Li metal induces poor wettability of Li_{BCC} on carbon that leads to nucleation overpotentials. Lithiophilic nanoseeds onto CNFs can guide Li_{BCC} deposition into CNFs and retard the growth of Li dendrite. By a combined electrospinning and Joule heating process, Yang et al. anchored silver nanoseeds on the CNFs that could direct Li deposition owing to its appreciable solubility in Li (Ag–Li phase diagram), hence yielding a dendrite-free Li anode.^[73] Guided by Ag nanoparticles, Li preferred to deposit on the CNFs_s with free Li dendrite. Without the Ag nanoseeds, however, Li dendrite would form on the CNF matrix due to irregular Li deposition. Using Ag-doped CNFs as the Li_{BCC} host, a highly stable Li metal anode was obtained with a low overpotential and long cycle life, enabling safe and high-energy Li metal batteries.

3.3. Developing 3D Nanofillers for Polymeric Solid Electrolytes

Compared with liquid electrolytes, polymeric SEs significantly enhance the safety and electrochemical stability in Li-based batteries, with great potential for safe, high-energy, and long-life batteries.^[7a,74] Moreover, polymeric SEs show good contact with the Li metal electrode compared with ceramic SEs, alleviating the increase of polarization of batteries. But current polymeric SEs have a severe problem of low Li^+ mobility, hence limiting their practical application.^[75] A large number of efforts have been made to disperse ceramic nanoparticles into a polymer matrix to enhance ionic conductivity and mechanical integrity.^[76] However, this method has its limitations, for the reason that Li ions need to cross many particle–particle junctions. Thus, the ionic transport pathway between 0D nanoparticles in polymeric matrix needs to be changed. 1D fiber fillers dispersed in polymeric SEs can afford many continuous ionic transport pathways through the fibers, greatly decreasing the cross-junction when compared to particle fillers. Combining the electrospinning technique with heat treatment is often used for the preparation of 1D ceramic SEs that are embedded into a polymer SE matrix. Liu et al. synthesized 1D $\text{Li}_{0.33}\text{La}_{0.557}\text{TiO}_3$ (LLTO) nanofibers by electrospinning their corresponding precursors, followed by calcination in air.^[77] The LLTO nanofiber-filled PAN/ LiClO_4 hybrid SEs showed an outstanding ionic conductivity up to $2.4 \times 10^{-4} \text{ S cm}^{-1}$ at room temperature. In addition, the electrochemical stability window of fiber-filled polymeric SEs was also enlarged. Fu et al. recently reported a flexible polyethylene oxide (PEO)-based membrane with 3D garnet-type $\text{Li}_{6.4}\text{La}_3\text{Zr}_2\text{Al}_{0.2}\text{O}_{12}$ (LLZO) fiber networks for Li metal batteries using a similar process (Figure 9b).^[78] The obtained flexible organic/inorganic SEs displayed a high ionic conductivity up to $2.5 \times 10^{-4} \text{ S cm}^{-1}$ at room temperature. The LLZO-filled PEO-based SEs blocked Li dendrite growth in symmetric Li/SE/Li half-cell during Li plating/stripping for about 500 h at 0.2 mA cm^{-2} , making them a promising platform for high-energy Li-based batteries.

3.4. Developing Flexible Membranes as Separators and Electrodes

Electrospun polymer porous membranes can also serve as flexible separators for batteries. The separators should integrate the

polymer matrix and the liquid electrolyte to provide paths for Li ion transportation (ionic conductive), while they should also be electronically insulating and thermo-mechanically strong to prevent two electrodes from touching, even in accident scenarios. Various polymers have been explored to produce the electrospun separators, which include PAN, PEO, polyvinylidene difluoride (PVDF), and polyvinyl chloride (PVC).^[79] For electrospun separators, sufficient amorphous regions of the polymer could help absorb the liquid electrolyte to provide excellent Li-ion conductivity. Moreover, the mechanical merit of the polymer is beneficial to reduce electrolyte leakage while maintaining the flexibility.^[80]

Specifically, for Li-S batteries, the electrospun membranes, working as a reservoir to assimilate the liquid electrolyte, could form a gel polymer electrolyte that would enable a high Li ion conductivity close to that of the liquid electrolyte. Meanwhile, the gel polymer electrolyte forms a physical passivation barrier layer on the sulfur electrode. It could suppress the diffusion of polysulfide, and thus block the polysulfide “shuttle effect” during cycling.^[79c,81] For instance, Wang et al. fabricated an electrospun polyimide (PI) nanofiber separator combined with a hot pressing process.^[79c] They found that because of the interconnected pore structure and sufficient polar-functional groups of the polymer macromolecules, which enabled strong chemical/physical adsorption or interactions, the diffusion of polysulfide would be inhibited. The loss of polysulfide for the “shuttle effect” was thus suppressed, with a capacity fade of only 0.08% per cycle during cycling. Moreover, to further prevent the “shuttle effect” of the polysulfide, organic and inorganic doping can be introduced into the electrospun polymer separators, which sometimes also helps increase the lithium ionic conductivity and reduce the interfacial impedance.^[82] Zhu et al.^[82b] doped SiO₂ nanoparticles onto PAN nanofibers to produce a multi-functional PAN/SiO₂ nanofiber separator. Compared to the separator without SiO₂ doping, they found that the doping of SiO₂ nanoparticles was not only favorable for fast Li ion diffusion attributed to the good electrolyte uptake capability, but was also helpful in mitigating the “shuttle effects” due to the role of the SiO₂ nanoparticles working as the absorption agent for polysulfide to suppress its transport.

Electrospun polymeric separators also demonstrate superior performance when applied for the lithium-metal batteries or LIBs.^[83] Study on electrospun PVDF-based separators for lithium-metal battery showed that after heat treatment at 160 °C, the softened PVDF fibers could form an interconnected framework to improve their physical properties. It presented a much better cycling ability with little capacity degradation after 50 cycles at 0.5C rate in comparison with the Celgard separator (PP separator)^[83a] due to the interconnected web structure made of the polymer fibers of nanoorder diameters. For LIBs, for example, the electrospun porous PVDF fiber-based separator showed a high ionic conductivity of 1.0×10^{-3} S cm⁻¹, also attributed to the fine interconnected web structures, when compared to the traditional commercial separators of microporous membranes, whose performance would be reduced by the low porosity and poor wettability.^[83b] Electrospun separators can also be made nonflammable by simply incorporating with some heat-resistant components. For example, a mixture of PAN and

heat-resistant ammonium polyphosphate (APP) could be electrospun to a hybrid separator that warrants battery stability at high temperature.^[84]

The electrospun nanofiber membranes can also be used as the freestanding flexible electrodes. This is of practical significance if flexible energy storage devices are to be applied for smart clothing, soft portable electronics with roll-up displays or wearable electronics.^[85] Electrospinning is powerful to produce flexible electrodes via various synthetic approaches as introduced in the preceding context. Thus, the electrospun fibers/tubules with diameters of few hundreds of nanometers can connect with each other to form a flexible 3D framework with good electronic conductivity. The excellent corrosion and fatigue resistance render the framework suitable for frequent use as flexible electrodes. A variety of flexible electrodes have been prepared for energy storage systems, for example, hybrids of SiO_x/Si nanotube, MoO₂/carbon, TiO₂/carbon, and MoS₂/carbon.^[47b,86] These electrodes present high mechanical flexibility, good conductivity, and with battery tests, they exhibited excellent rate capability and cycling stability.

4. 1D Electrospun Nanomaterials as Nanoreactor for In Situ TEM

In situ TEM technique is a powerful tool that allows for real-time examinations of material formation and reaction processes.^[87a] Electrospun nanofiber itself, due to electron transparency, easy mechanical manipulation, and prepositioning of chemical ingredients by liquid solution mixing, is an ideal nanoreactor, from which we can directly observe its material synthesis process by in situ TEM characterization. The nanofiber diameter is usually from tens to around a few hundred nanometers. This is easy for TEM users to search the sample and locate the reaction sites during the synthesis. By using 1D electrospun nanomaterials as the nanoreactor for in situ TEM study, it enables a much better basic understanding of the detailed mechanisms of materials synthesis and properties. These features are rather similar to how carbon nanotubes have historically boosted the development of the in situ TEM approach, and nanoscience in general.^[87b,c]

4.1. Characterizing Synthesis Process of Porous Nanomaterials

4.1.1. Carbonization of Precursors

The carbonization process of the prepared electrospun polymers could be investigated by applying in situ heating TEM experiments. For example, the synthesis of CNFs involves the carbonization of their precursors of electrospun PAN nanofibers. Owing to the high elongation forces by the applied voltage, the electrospinning process would induce a high orientation of polymer chains, and thus could enhance the crystallinity of CNFs after the carbonization.^[88] For the carbonization, PAN nanofibers are first stabilized at 230–280 °C and then heated at an elevated temperature of 1200–3000 °C to form CNFs^[89] The graphitization process of PAN has been theoretically proposed with the structural schematics

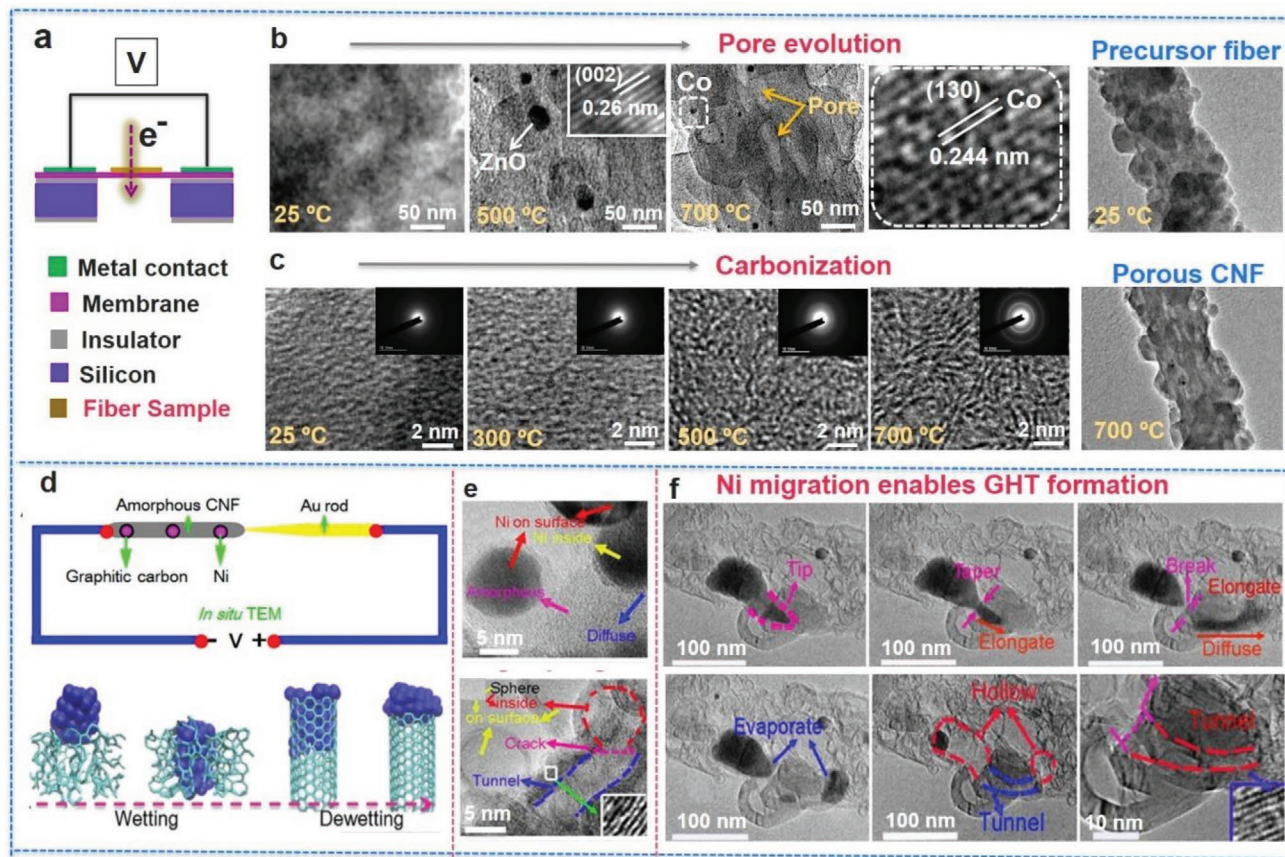


Figure 10. a) Schematic setup of in situ TEM heating stage for heat treatment of fiber precursors, b) pore evaluation and c) carbonization of bimetallic MOFs (ZIF-8 and ZIF-67). Adapted with permission.^[56] Copyright 2017, Elsevier. d) Schematics of CNF matrix for Ni migration under in situ TEM setup. e) Hollow structure created by Ni⁰ migration and evaporation after Joule heating. f) Detailed process of Ni⁰ nanoparticle migration inside CNF matrix for the formation of GHT structures. Adapted with permission.^[14a] Copyright 2017, Elsevier.

linked to the corresponding carbonization steps.^[90] However, direct observations are required to confirm the processes. An in situ TEM experiment with heating was performed to study the graphitization of PAN by Prilutsky et al., from which the crystallization temperature for PAN was observed and verified.^[91] PAN was observed to be carbonized to amorphous carbon at ≈ 500 °C, with only two or three stacked short graphene nanosheets formed in the amorphous carbon matrix. With increasing temperature, no obvious graphitization of amorphous carbon was seen until the temperature reached ≈ 750 °C, when the noticeable enhancement of orientation (i.e., more crystallization) of amorphous carbon could be observed. Furthermore, when the temperature was increased to 900 °C, the orientation appeared to reach the maximum and did not change much with longer heating time. Conversely, it was also found from in situ TEM observations that the introduction of CNTs into the PAN nanofibers could further enhance the graphitization degree of carbon from PAN during carbonization. The PAN chains adjacent to the CNT wall were observed to be preferentially converted into graphitic layers, which followed the curvature of CNTs.

Moreover, this tool can also monitor the carbonization process for the other precursors, such as bimetallic MOFs (ZIF-8 and ZIF-67).^[56] The prepared samples were amorphous when

the temperature was increased from 25 to 300 °C without any graphene layers observed (Figure 10c). From 300 to 500 °C, the bimetallic MOFs would be carbonized to amorphous carbon with few layers of stacked graphene nanosheets, showing the initial graphitization at this stage. The carbon exhibited enhanced graphitization with further increase of temperature to 700 °C. In addition to the observation of the carbonization of bimetallic MOFs, several typical chemical reactions during this process were observed. It was found that Zn from ZIF-8 could react with Co from ZIF-67 to form Zn-Co alloys including Zn₃Co and Zn₁₃Co. At high temperature, Zn₃Co was not stable and decomposed into Co and Zn₁₃Co. Carbonization of bimetallic MOFs was monitored to yield graphene-layer-containing carbonaceous materials with Zn, Co, and Zn₁₃Co inside. While Zn would be evaporated at higher temperature, Co could serve as catalyst to further promote the graphitization degree.

4.1.2. Pore Evolution

Chemicals like KOH and ZnO can etch carbon at high temperature to create pores in the resulting sample, but the detailed process is still unclear. To unravel the whole etching process,

Chen et al. added $\text{Zn}(\text{Ac})_2$ in electrospun PAN nanofibers for in situ TEM observation (Figure 10a,b).^[56] An in situ heating TEM stage that controls the temperature from 25 to 700 °C was used to investigate the whole dynamical process from the electrospun precursor to the porous CNFs. The sample showed almost identical feature to the original when heated at 300 °C. With further increase of temperature to ≈ 500 °C, PAN was observed to convert to carbon decorated with some black nanoparticles due to the decomposition of the precursor. High-resolution (HR)TEM analysis showed that these particles with an interplanar distance of 0.26 nm would be ascribed to the (002) plane of ZnO, showing the conversion of ZIF-8 to ZnO at 500 °C. The formed ZnO etched the carbon to form a porous structure when the temperature was further increased to 700 °C, creating a porous carbon.

4.1.3. Graphitic Hollow Tunnel (GHT) Formation through Ni^0 Migration

The synthesis of hollow graphitic nanocarbons is significant for many applications from catalyst supports to gas storage materials.^[92] Several methods have been widely used to prepare these carbons with several inherent challenges.^[93] Further development of new methods for their synthesis is necessary. We developed the Ni^0 migration method to in situ create the graphitic hollow tunnel (GHT) structures in carbon matrix.^[14a] But the detailed process of Ni^0 migration is not well understood (Figure 10d). To examine the mechanism, we performed an in situ TEM technique to study the whole process of Ni^0 migration using electrospun Ni/carbon composite nanofibers, where Ni^0 nanoparticles were encapsulated in electrospun amorphous CNFs.^[15a] A single electrospun Ni/carbon nanofiber for observation was attached to a gold rod to form a circuit and the temperature of the sample could be increased based on Joule heating. We conducted an exploratory experiment using Ni^0 nanoparticles with $\approx 5\text{--}10$ nm diameter. After Ni^0 migration, we clearly saw a tunnel structure, verifying the feasibility of the designed experiment (Figure 10e). However, a small Ni^0 particle migrated and shrunk very quickly within 1.0 s, and it was difficult to record the whole process. Alternatively, a large Ni^0 particle was selected to address this issue. Following the Joule heating treatment, the large Ni^0 particle started to evaporate but part of it got attached and migrated continuously into the surrounding amorphous carbon, yielding an elongated Ni^0 tip, which then broke apart from the maternal Ni^0 nanoparticle. The separated Ni^0 particles still stretched and migrated continually. As the Ni^0 particles continuously etched the amorphous carbon through the movement paths, a hollow tunnel with graphitic walls was observed due to the Ni^0 -catalytic conversion from amorphous carbon to graphitic carbon. Finally, the Ni^0 particle completely vanished, producing a pure graphitic hollow tunnel inside the CNF (Figure 10f). The driving force for the process was attributed to the high temperature induced by Joule heating and Ni^0 -catalytic transformation of amorphous carbon into more stable graphitic carbon.^[94] In situ TEM experiments showed a detailed etching-elongation-contraction process, accompanied by the evaporation of Ni^0 particles.

Based on the above in situ TEM results, molecular dynamics simulation was further conducted to study the detailed mechanism of Ni^0 migration (Figure 10d). Due to active dangling bonds on amorphous carbon surface, the calculated adhesion between the Ni^0 surface and amorphous carbon was much stronger than that between the Ni^0 surface and perfect graphene. This strong adhesion would drive a Ni^0 particle penetrating inside amorphous carbon to create a hole, as the energy of the whole system kept dropping upon the wetting process. The Ni^0 particle inside the amorphous carbon would induce a structural evolution (graphitization) of the hole wall.^[95] As a consequence of graphitization, the Ni^0 particle was surrounded inside a high-quality GHT, and the Ni^0 particle would be expelled to migrate to the outside of the GHT. This dewetting procedure was due to the low adhesion between high-quality graphitic wall and Ni^0 . Through in situ TEM and modeling, a new mechanism for the GHT formation induced by Ni^0 migration was revealed and called the wetting-to-dewetting transition.

4.2. Characterizing Electrochemical Reaction Behavior

During charging and discharging, the electrode materials of batteries undergo electrochemical reactions, such as lithiation/delithiation and sodiation/desodiation. These electrochemical reactions also accompany structural and compositional evolutions of the electrode materials, which affect the capacity and cycling stability for battery performance.^[96] The understanding of these evolutions is important and help optimize the battery electrodes. This can be achieved by characterization using the in situ TEM technique which allows the whole process during the electrochemical reaction with morphology and structure changes to be observed and recorded.^[87,97] For in situ TEM observations, the electrospinning technique is very convenient to tune and prepare different kinds of porous nanostructures, e.g., from small-diameter carbon nanofibers or nanotubes to more complex hybrids, all of which can act as an electrochemical nanoreactor in an in situ TEM nanobattery set-up. This capability is helpful to understand the electrochemical reaction processes of battery materials with different architectures. In the subsections below, several typical electrospun nanomaterials as electrochemical nanoreactors for in situ TEM study of battery materials are outlined and described.

4.2.1. Anodes of Li-Ion Batteries

Anode materials such as Sn and Si have been extensively investigated for LIBs in view of their high capacities. However, the fast fading of capacity due to the large volumetric change upon lithiation–delithiation reaction leads to short cycling life of the battery. Loading these anodes into stable and rigid substrates with porous/hollow structure can accommodate their large volume change. Here, for example, various porous Si/carbon composites^[98] have been prepared by the combined single- or coaxial-nozzle electrospinning and calcination process. To uncover the Si lithiation/delithiation process with

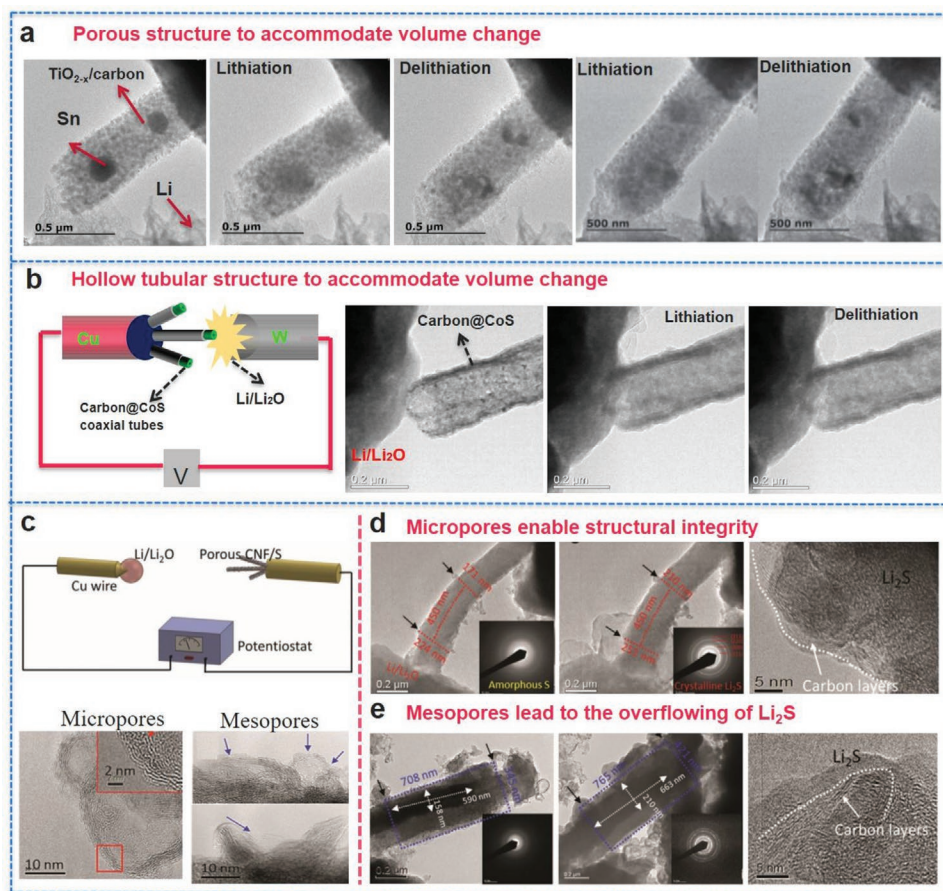


Figure 11. a) Electrospun TiO_{2-x} -carbon matrix for in situ TEM setup to study the lithiation/delithiation process of Sn. Adapted with permission.^[100] Copyright 2016, Wiley-VCH. b) Carbon hollow tubules as in situ TEM host for the lithiation/delithiation process of CoS. Adapted with permission.^[55] Copyright 2016, Wiley-VCH. c) Schematic of in situ TEM setup for sulfur cycling inside porous CNF matrix. Lithiation of sulfur inside CNFs with d) micropores and e) mesopores. Adapted with permission.^[101] Copyright 2017, Wiley-VCH.

carbon matrix, Wang et al.^[99] used electrospun CNFs as the nanoreactors, which were either attached with Si nanoparticles or encapsulated Si nanoparticles, for the in situ TEM study. They observed that the aggregated Si particles on the surface of CNFs showed contact flattening during initial lithiation. However, the Si nanoparticles inside the CNFs exhibited delayed lithiation when compared to those on the CNF surface. Lithiation of Si particles inside the CNF generated a high stress field, which would cause it to fracture. Therefore, the design of Si-based composites needs to consider not only the stability of the matrix but also the introduction of porosity to accommodate the large volume change upon cycling. In addition to Si, Sn could also combine with porous robust materials to form a hybrid structure to achieve higher mechanical integrity.

Besides carbon, carbon/ TiO_2 hybrid nanofibers prepared by electrospinning-based approach also exhibit porous structures with good mechanical robustness. For synthesis, $\text{Ti}(\text{OiPr})_4$ -PS-tin(II)₂-ethyl hexanoate was first electrospun to form the composite fibers by Li et al. (Figure 11a).^[100] Further by a two-step heat treatment, the electrospun precursor was then converted to robust porous 1D TiO_{2-x} -C composite nanofibers, whereby Sn nanoparticles were encapsulated inside. When building up

the nanobattery set-up with the hybrid composite as anode for in situ TEM experiment, it enabled observation of the structural evolution of Sn in the porous TiO_{2-x} -C nanofibers upon cycling. During the initial lithiation, Sn nanoparticles suffered from obvious volume expansion, but the pores around these Sn particles could accommodate their expansions. No volume change of the lithiated TiO_{2-x} -C composite nanofiber matrix was observed, confirming the excellent mechanical property of the electrospun TiO_{2-x} -C composite matrix. In the delithiation processing, the original Sn particles were separated into many small subparticles, mainly due to the surface absorption forces between matrix and the Sn particle. However, these smaller Sn subparticles were still well located and attached to the pores in the matrix which would accommodate their large volume changes in ensuing cycles. Batteries constructed from these porous TiO_{2-x} -C-Sn composite nanofibers manifested a high capacity of 957 mAh g^{-1} at 0.1 A g^{-1} and an ultralong life well over 10 000 cycles with $\approx 18\%$ capacity fading. This simple method offers new avenues for other anode materials, which suffer from large volume expansions. The in situ TEM study has also demonstrated that the hollow carbon tubules as a matrix could also maintain the structural integrity for active anode materials (CoS_x , Figure 11b).^[55]

4.2.2. Sulfur Cathode of Li–S Batteries

The structural parameters for the sulfur hosts are critical for the electrochemical performance of Li–S battery. For example, what is the appropriate pore size? Large pores can provide more space to store sulfur and accommodate the volume change upon cycling. However, if the pores were too large, the polysulfide formed during lithiation may flow out from these pores into the electrolyte, losing the sulfur active materials. Besides these, there are also other questions, such as the structural stability of the sulfur hosts during cycling, and the polysulfide dispersion in the porous hosts. The understanding of these details really matters and can guide the fundamental design of the structure for S hosts for better Li–S batteries. Xu et al.^[101] (Figure 11c) used a combined electrospinning and template technique to prepare electrospun porous CNFs with two different pore sizes of mesopores and micropores for sulfur storage. They built an in situ TEM nanobattery by using these porous CNFs to observe the electrochemical processes of sulfur cathode. For the CNF with micropores (Figure 11d), the recorded TEM images displayed the uniform lithiation process over the whole nanofiber, and the selected area electron diffraction (SAED) pattern confirmed the conversion from amorphous sulfur to crystalline Li₂S nanoparticles with 10–20 nm after full lithiation. It is also noted that the porous CNF remained unexpanded along the fiber direction after full lithiation, while the diameter of the porous CNF expanded with a volume expansion of 35% which is much lower than the theoretical expansion of sulfur (80%). The smaller expansion would be due to the robust graphitic carbon layers that significantly limited the expansion of Li₂S, and the pores that could accommodate the volume expansion. The porous CNFs with micropores showed excellent structural stability when used as a sulfur host for Li–S batteries.

When compared to porous CNFs with micropores, these porous CNFs with mesopores showed three key differences (Figure 11e): the sublimation of sulfur, the larger volume change, and the overflowing of Li₂S. With in situ TEM examination, after lithiation, Li₂S was observed on the outer surface of these porous CNFs, indicating that the graphitic hollow carbon spheres with diameter of 8 nm (mesopores) in CNFs were unable to avoid overflowing of Li₂S. This was because the molecular size of Li₂S was only ≈0.5 nm, so that Li₂S molecules could overflow through these mesopores. However, carbon hollow spheres with 0.54 nm (micropores) would confine Li₂S and prevented its overflowing by the physical barrier. The CNFs with mesopores suffered from larger volume expansion in both diameter (from 158 to 210 nm) and length (from 590 to 663 nm) directions after full lithiation. The volume expansion reached 98%, which was much larger than 35% for CNFs with micropores and the theoretical expansion of 80% for sulfur, mainly due to the expansion of Li₂S out of the porous CNFs.

Coin cell tests showed that when using CNFs with mesopores as the sulfur hosts, the carbon/sulfur composite electrode not only gave poor mechanical stability but also yielded ill confinement of Li₂S during lithiation, leading to poor cycling stability of the Li–S batteries. However, the CNFs with micropores with a sulfur loading of 71% showed a high

capacity of 945 mAh g⁻¹, and exceptional high-rate capability and cycling stability.

But it should be noted that such in situ TEM nanobattery was not totally identical to the real coin cell battery with liquid electrolyte. There are two major issues that remained with this nanobattery set-up: i) the electrode/electrolyte interface is different from that in a practical battery with liquid electrolyte and ii) the direct conversion from S to Li₂S phase without the generation of long-chain and short-chain polysulfide. Due to these two problems, it is difficult to understand all the details of the electrochemical process and the evaluation of the stability of porous carbon as the sulfur host may not be fully accurate. Further work is required to design an electrospun fiber-based nanobattery with liquid electrolyte.

4.2.3. Li Metal Anode of All-Solid-State Li Metal Batteries

All-solid-state Li metal batteries have been considered as a promising next-generation power system. However, solid-state Li metal batteries suffer from several severe challenges such as adhesion between SE and Li metal, electrochemical stability of SE against Li metal, and large electrochemically generated stresses inside the Li metal. Using the porous Li metal hosts is a promising solution to address these problems, however, the detailed behavior and dynamic process of Li plating/stripping inside the hosts need to be clarified. The in situ TEM technique combined with the use of the prepared electrospun Li hosts as nanoreactors could enable the direct observations of Li plating/stripping process in order to explore its kinetics and mechanisms.

Current cryo-TEM technique is not capable of in situ observation of Li plating/stripping. Investigation of the electrochemical process of Li plating/stripping by in situ TEM is also challenging due to the electron beam damage on Li metal.^[102] Moreover, as a very light element, lithium has a very low contrast for TEM imaging, which can be easily blurred by the contrast from Li hosts made of heavier elements. It is urgent to find a suitable way to reduce the electron beam damage and keep the contrast from Li metal observable to achieve in situ characterization of Li plating/stripping. A breakthrough on this topic was made in our work (Figure 12).^[15b] We developed an in situ TEM technique to study the detailed mechanism of Li plating/stripping by using porous CHTs which were prepared by a combined electrospinning and etching process as mentioned in Section 3.1 (Figure 12a). The existence of the CHTs, as an encapsulation layer surrounding the Li metal, helped relieve the radiation damage. With Li plating inside the tubule, the CHT encapsulation helped to reduce the sputtering damage led by elastic interactions of the electron-nucleus scattering. For inelastic scattering of electron–electron scattering, the CHT would also act as the thermal/electron conductor covering on the plated Li to release some heat by electron irradiation. Moreover, the CHT wall was thin and porous, possessing a very low mass-thickness contrast, thereby allowing Z-contrast from Li metal inside CHTs to be clearly observable.

The in situ TEM characterization was realized with a Nanofactory scanning tunneling microscope (STM)/TEM holder using a JEOL 2010F TEM at 200 kV. Our nanobattery inside

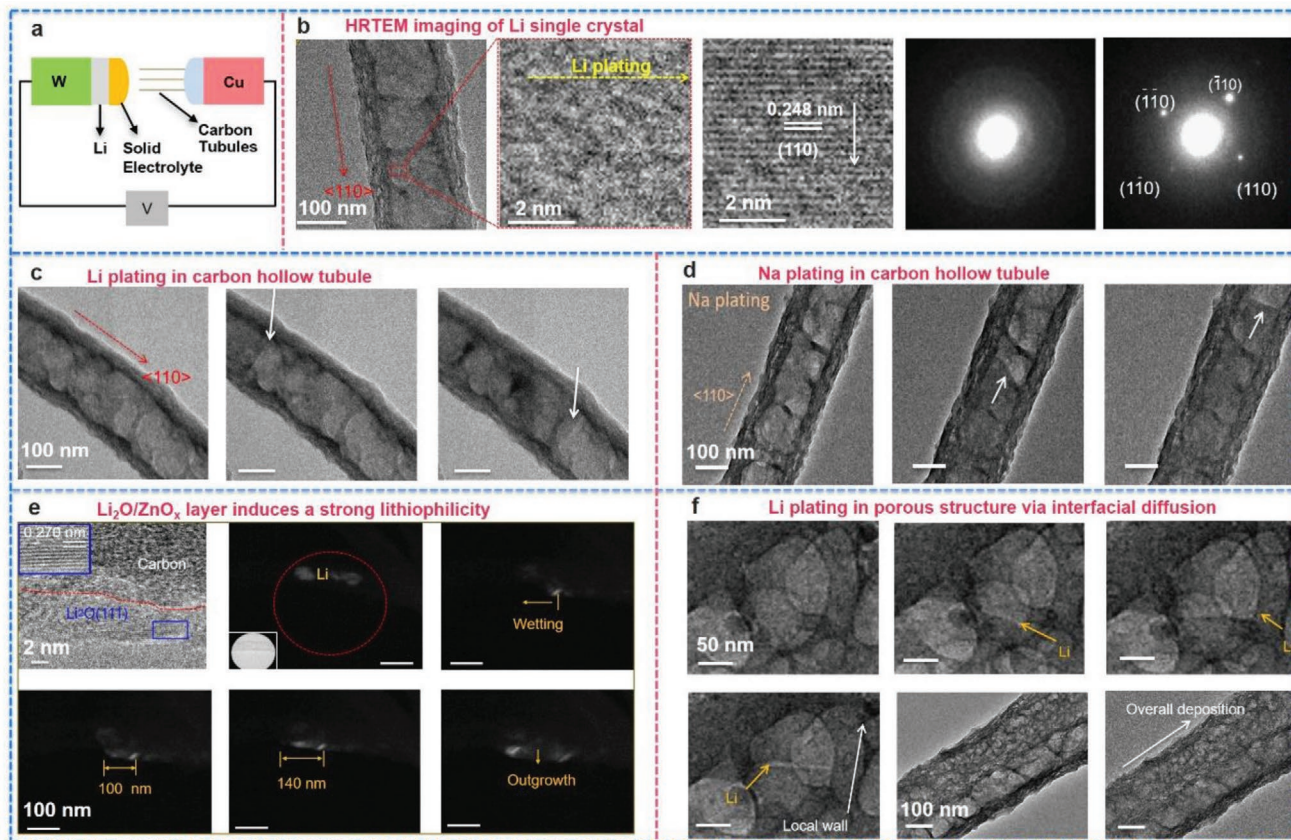


Figure 12. a) Schematic of in situ TEM setup using carbon hollow tubes as a Li host. b) HRTEM imaging of Li single crystal plating. TEM imaging of c) Li plating and d) Na plating inside carbon hollow tubes. e) Lithiophilicity induced by ZnO_x . f) Li plating inside pores of CNFs. Adapted with permission.^[15b] Copyright 2020, Springer Nature.

the in situ TEM comprised PEO-based composite as SE, CHTs as the Li host, and the counter electrode of Li metal. The SE-coating Li metal was placed in contact with CHTs to form an electrochemical cell (Figure 12a). A slightly under focused condition was used to enhance the contrast, and limited experiment recording time was applied to reduce the influence from beam damage. Li plating/stripping process in CHTs was realized by applying ± 2 V versus Li/Li⁺. The CHTs were first lithiated to form mixed ionic-electronic conductors (MIECs) for Li plating/stripping, and ZnO_x was also introduced and uniformly distributed into CHTs to enhance the lithiophilicity of the CHT wall (Figure 12c). It was found that Li plating with a dark contrast underwent tip growth, filling inside and could grow along the tube over 6 μm length like an “incompressible fluid.” SAED analysis on the tube region showed that when Li plating occurred, it was featured as a nearly single crystal pattern. HRTEM imaging showed a fresh Li crystal with 0.248 nm lattice spacing between (110)_{Li} lattice fringes which are normal to the tube axis (Figure 12b). More importantly, reversible Li plating/stripping was also observed in aligned double-CHTs and triple-CHTs. Each tube would direct Li deposition/stripping along the tube simultaneously without affecting other tubes, illustrating that a Li meal hydraulic engine was possible at a single “pipe” or few-“parallel pipes” level, and the “atomic fountains” of pure Li metal was established inside the

CHTs. The tests of cycling stability of CHTs by in situ TEM were also performed and indicated that the prepared materials would maintain their mechanical integrity even after 100 cycles of reversible Li plating/stripping.

Experiments and theoretical modeling confirmed that the dominant mechanism for Li plating/stripping inside CHT was the Coble creep through interfacial diffusion via the phase boundary between the Li metal and the MIEC wall (Figure 13). When 3D obstructions of the MIEC structures were created inside the tube, smooth Li deposition/stripping was also observed by interfacial diffusion along the MIEC/Li interface (Figure 12f). Carbon hollow tubes with inner-diameters from 30 to 200 nm were also tested and showed good mechanical properties without degradation after cycles of Li metal plating and stripping. More importantly, the Coble creep mechanism via interfacial diffusion uncovered in the solid-state lithium metal battery was actually a general mechanism for the plating/stripping of other alkali metals. Sodium was used as an example to show that it would also extend to other alkali metals. In sodium metal nanobatteries, the sodium metal would also flow and retract inside the MIEC channel as a single crystal. The dominant mechanism for sodium plating/stripping inside CHT was also the Coble creep diffusion through the phase boundary between the Na metal and the MIEC wall (Figure 12d).

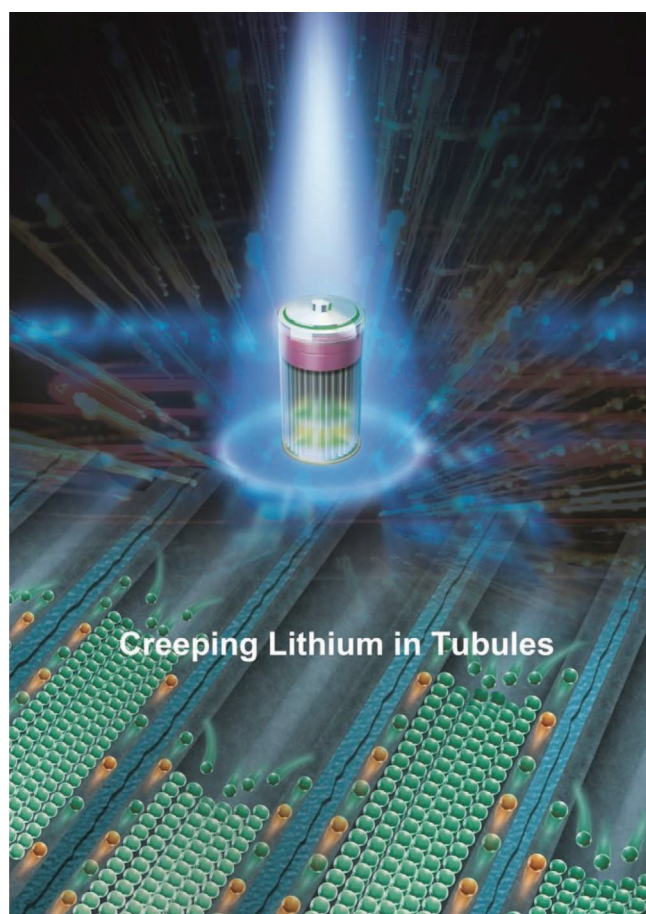


Figure 13. Schematic of the mechanism of Li plating/stripping via Coble-creep by interfacial diffusion via the phase boundary between Li metal and the prepared electrospun MIEC tubule wall.

Moreover, the in situ TEM method can be applied to study the lithiophilicity mechanism of additives such as ZnO_x . Here, ZnO_x was introduced and uniformly distributed in the prepared electrospun CHT walls. During lithiation, Li_2O could be produced by ZnO_x . However, it is very difficult to conduct TEM imaging on post-formation Li_2O directly due to limited amount of Li_2O (\approx nm thickness) and its location inside CHTs. We used an alternative way to examine the in situ formed Li_2O that also appeared on the outer surface of CHTs, since ZnO_x was uniformly decorated in the CHT wall. A nanocrystalline Li_2O layer, like a lubricant, was observed on the tubular outer surface after lithiation (Figure 12e). By overplating Li inside CHTs, Li plating could transport through the nanopores on the porous CHT walls and appear on the outer surface of the CHTs. It was interesting to observe that after plating through the nanopores, Li metal first underwent complete wetting and then spread along the outer surface up to a distance of 140 nm with zero contact angle, suggesting that the $\text{Li}_2\text{O}/\text{ZnO}_x$ layer on outer surface of MIEC helped induce strong lithiophilicity. The electrochemical performance for Coble-creep enabled all-solid-state Li batteries showed that the batteries with MIECs as the Li metal host manifested much better performance than control experiments without MIECs.

Thus, studies combining materials theory and in situ TEM technique with 1D electrospun nanoreactors can play a significant role in advancing our basic knowledge of alkali metal plating/stripping mechanisms and providing guidance on the practical solutions for all-solid-state alkali metal batteries.

5. Summary and Outlook

In this review article, we have introduced the basic electrospinning technique and its association with other approaches such as CVD, hydrothermal method, etc., to enable the synthesis of hybrid nanoframeworks with various architectures and compositions for battery materials. By focusing on controls of the combined strategies, we have provided some insights on the nanostructural engineering mechanisms and on the electrochemical performance. In this context, we have concluded several unique applications facilitated by the electrospinning-based strategies, such as the constructions of carbon tubular networks for battery electrodes, the hollow Li and sulfur nanohosts with tailored structural and compositional features, the fiber-filling polymeric solid-state electrolytes, and the multifunctional flexible separators/electrodes made of electrospun nanofibers. Electrospinning also enables the setup of in situ TEM nanobatteries for characterization of battery materials, or work as 1D nanoreactors for understanding the synthesis processes.

The exceptional performance of the prepared electrospun materials is ascribed to several advantages. First, the nanostructured active materials enable sufficient contacts between active materials and electrolyte, which hence shorten the ion diffusion pathways and enhance the rate capability. Second, the electronic conductivity and structural stability of the electrodes can be enhanced significantly by introducing a robust carbon tubular network that is far more tolerant of changes than ad hoc percolations of, for example, conventional carbon black nanoparticles like Ketjenblack. Third, porous/hollow structures are of great significance in accommodating large volume change of electrode materials, especially for Li metal and sulfur, thus promising a long-term cycling life. Meanwhile, for Li-S batteries, these porous structures can efficiently block dissolved polysulfide by physical/chemical bonding and maintain the structural integrity to acquire long cycling life.

Electrospinning is an efficient and versatile approach to prepare advanced nanomaterials with hierarchical structures as electrode materials (Table 2), separators, and electrolytes for energy storage applications. In electrospinning, the fiber generator is very important in large-scale fiber production. Multinozzle electrospinning shows higher throughput than the traditional single-nozzle counterpart because it can enable many jets simultaneously, yielding more materials. Reasonable design of internozzle distance is the key to decrease the edge effect caused by multijet interferences. Besides multinozzle electrospinning, needleless electrospinning and bubble electrospinning are two other available selections which can enable many Taylor cones to form a large number of jets at the same time. For example, in bubble electrospinning, the gas pump with compressed gas is used to create the bubbles in the electrospinning solution on the nozzle tip to induce the Taylor cone. One nozzle is able to form many bubbles determined by

Table 2. Comparison between electrospun 1D carbon-based materials and those derived from other competing synthetic techniques.

	Electrospinning	Hydrothermal	CVD	Templating
Mass production	Easy	Hard	Easy	Hard
Cost	Relatively low	High	High	High
Processing	Simple	Relatively simple	Simple	Complex
Tuning diameter	Easy (10 nm to 10 μ m)	Hard	Relatively hard	Easy
Flexible/freestanding (starting from precursors)	Easy	Hard	Hard	Hard
In situ incorporation with other materials	Easy	Easy	Hard	Hard

the nozzle diameter and the gas pressure. However, in needleless electrospinning, various fiber generators, including bowel edge and rotary cone in the open liquid surface, also allow the electrospinning solution to form plenty of liquid jets simultaneously. These developed electrospinning techniques show great capability for mass production of electrospun materials. To reduce the synthetic costs of materials, a main method is to recycle the organic solvents. Currently, recycling of solvents is largely realized through the condensation technology. Some electrospun products have already been commercialized and used in energy storage applications such as separators (e.g., Jiangxi Advanced Nanofiber S&T Co., Ltd). With further development of the electrospinning techniques, many more electrospun products will be commercialized in the next decade.

Electrospinning-based strategies enable a powerful and versatile technique with a broad range of applications. Not only can it be used to prepare advanced materials as electrodes, separators, and nanoreactors for batteries, but also serve in other fields like chemical separation and tissue engineering. In parallel with recent advances on R&D of electrospinning, the engineering applications of electrospun nanofibers have been continuously expanding. Some products based on the electrospinning technique have reached the market place, for example, battery separators, air filtration (e.g., masks, industrial filter papers, and antimog window screens), ultrafiltration membrane materials for water filtration, and waterproof and moisture-permeable fabrics. In addition, there are also many products which can be readily commercialized such as those for sensing and detection, oil–water separation, tissue engineering scaffolds, insulation materials, etc.

Despite the aforementioned developments of the electrospinning-based strategies for advanced nanomaterials synthesis and as a nanoreactor for in situ characterization, several significant challenges still remain, awaiting future efficient solutions associated with innovative techniques. These are:

- i. Durability and flexibility. Hydrothermal method is usually used to grow active materials (metal oxide, metal sulfide, etc.) onto electrospun carbon nanofibers/nanotubes to form hybrids with high conductivity. Unfortunately, these active materials on the electrospun carbon matrix still suffer from degradation because their volume change cannot be fully accommodated. The flexibility of these composites will also be correspondingly reduced. Coating a stable material (carbon, etc.) onto these active materials through other methods, such as CVD and sputtering, could possibly combat these issues.
- ii. Mass production. Although mass production of nanofiber films has been reported by multinozzle electrospinning, some of the other associated techniques (e.g., hydrothermal method) used for the functionalization of these electrospun films remain difficult to scale up for mass production.
- iii. Complex fabrication. In some cases, several different techniques are combined to prepare 3D hierarchical architecture with unique structural and compositional advantages. The synthetic method to fabricate these materials, however, is relatively complex. It is imperative to develop novel but simple design routes of synthesis. One direction is to integrate different methods in a single step.
- iv. Electrospun nanomaterials as nanoreactor. The electrospinning technique is efficient to arrange various precursors into 1D nanomaterials as a nanoreactor for in situ TEM study. In situ HRTEM imaging is very powerful to yield detailed structure information of the materials. However, this depends strongly on the diameter of the electrospun nanofibers. Modulations on some electrospinning conditions, e.g., by heating the electrospinning solution, could possibly further optimize the diameter of electrospun nanomaterials.

In summary, electrospinning-based synthetic strategies are developing rapidly and are expected to play a larger role in future energy storage technologies.

Acknowledgements

This work was financially supported by National Key Research and Development Project of China for Demonstration of Integrated Utilization of Solid Waste in Distinctive Convergent Areas of Southeast Light Industry Building Materials (2019YFC1904500), China's Central Government-guided Fund for Science and Technology Development to Local Governments (2019L3005), and Social Development Industry-University Research Cooperation Project from the Department of Science and Technology in Fujian (2018Y4002). X.Y.L. would like to acknowledge the support by the Award Program for Minjiang Scholar Professorship. J.L. acknowledges the support by Samsung Advanced Institute of Technology. Y.-W.M. thanks the support from the Australian Research Grants Council (DP130104648) for his work on electrospun polymer nanocomposites. Y.M.C. would like to thank Professor John B Goodenough for his guidance since 2013.

Conflict of Interest

The authors declare no conflict of interest.

Keywords

energy storage, hierarchical architecture, in situ TEM characterization, materials processing, nanoreactors

Received: March 4, 2020

Revised: May 7, 2020

Published online:

- [1] a) J. Qian, B. D. Adams, J. Zheng, W. Xu, W. A. Henderson, J. Wang, M. E. Bowden, S. Xu, J. Hu, J.-G. Zhang, *Adv. Funct. Mater.* **2016**, *26*, 7094; b) S. Dong, X. Chen, L. Gu, X. Zhou, L. Li, Z. Liu, P. Han, H. Xu, J. Yao, H. Wang, X. Zhang, C. Shang, G. Cui, L. Chen, *Energy Environ. Sci.* **2011**, *4*, 3502; c) S. Li, M. Jiang, Y. Xie, H. Xu, J. Jia, J. Li, *Adv. Mater.* **2018**, *30*, 1706375; d) L. Peng, Z. Fang, Y. Zhu, C. Yan, G. Yu, *Adv. Energy Mater.* **2018**, *8*, 1702179; e) X. Cao, H. Li, Y. Qiao, X. Li, M. Jia, J. Cabana, H. Zhou, *Adv. Energy Mater.* **2020**, *10*, 1903785; f) H. Wang, J. Hu, J. Dong, K. C. Lau, L. Qin, Y. Lei, B. Li, D. Zhai, Y. Wu, F. Kang, *Adv. Energy Mater.* **2019**, *9*, 1902697.
- [2] a) J. Zheng, M. H. Engelhard, D. Mei, S. Jiao, B. J. Polzin, J.-G. Zhang, W. Xu, *Nat. Energy* **2017**, *2*, 17012; b) K. J. Harry, X. Liao, D. Y. Parkinson, A. M. Minor, N. P. Balsara, *J. Electrochem. Soc.* **2015**, *162*, A2699; c) C. Zhao, L. Liu, X. Qi, Y. Lu, F. Wu, J. Zhao, Y. Yu, Y.-S. Hu, L. Chen, *Adv. Energy Mater.* **2018**, *8*, 1703012; d) Y. Li, J. Fu, C. Zhong, T. Wu, Z. Chen, W. Hu, K. Amine, J. Lu, *Adv. Energy Mater.* **2019**, *9*, 1802605; e) F. Zhao, J. Liang, C. Yu, Q. Sun, X. Li, K. Adair, C. Wang, Y. Zhao, S. Zhang, W. Li, S. Deng, R. Li, Y. Huang, H. Huang, L. Zhang, S. Zhao, S. Lu, X. Sun, *Adv. Energy Mater.* **2020**, *10*, 1903422; f) J. Wang, Y. Wang, D.-H. Seo, T. Shi, S. Chen, Y. Tian, H. Kim, G. Ceder, *Adv. Energy Mater.* **2020**, *10*, 1903968.
- [3] a) Y. Kato, S. Hori, T. Saito, K. Suzuki, M. Hirayama, A. Mitsui, M. Yonemura, H. Iba, R. Kanno, *Nat. Energy* **2016**, *1*, 16030; b) K. Sakaushi, E. Hosono, G. Nickerl, T. Gemming, H. Zhou, S. Kaskel, J. Eckert, *Nat. Commun.* **2013**, *4*, 1485; c) H. Wang, C. Zhu, D. Chao, Q. Yan, H. J. Fan, *Adv. Mater.* **2017**, *29*, 1702093; d) N. Wang, Z. Bai, Y. Qian, J. Yang, *Adv. Mater.* **2016**, *28*, 4126; e) D. Bin, F. Wang, A. G. Tamirat, L. Suo, Y. Wang, C. Wang, Y. Xia, *Adv. Energy Mater.* **2018**, *8*, 1703008.
- [4] a) L. Suo, W. Xue, M. Gobet, S. G. Greenbaum, C. Wang, Y. Chen, W. Yang, Y. Li, J. Li, *Proc. Natl. Acad. Sci. USA* **2018**, *115*, 1156; b) M. Gu, Y. He, J. Zheng, C. Wang, *Nano Energy* **2015**, *17*, 366; c) L. Hu, C. Dai, H. Liu, Y. Li, B. Shen, Y. Chen, S.-J. Bao, M. Xu, *Adv. Energy Mater.* **2018**, *8*, 1800709; d) Y. Pan, S. Gao, F. Sun, H. Yang, P.-F. Cao, *Chem. Eur. J.* **2019**, *25*, 10976.
- [5] a) T. Yang, B. Guo, W. Du, M. K. Aslam, M. Tao, W. Zhong, Y. Chen, S.-J. Bao, X. Zhang, M. Xu, *Adv. Sci.* **2019**, *6*, 1901557; b) C. Dai, L. Hu, X. Li, Q. Xu, R. Wang, H. Liu, H. Chen, S.-J. Bao, Y. Chen, G. Henkelman, C. M. Li, M. Xu, *Nano Energy* **2018**, *53*, 354; c) L. Hu, C. Dai, J.-M. Lim, Y. Chen, X. Lian, M. Wang, Y. Li, P. Xiao, G. Henkelman, M. Xu, *Chem. Sci.* **2018**, *9*, 666.
- [6] a) C. Dai, L. Hu, M.-Q. Wang, Y. Chen, J. Han, J. Jiang, Y. Zhang, B. Shen, Y. Niu, S.-J. Bao, M. Xu, *Energy Storage Mater.* **2017**, *8*, 202; b) B. Guo, T. Yang, W. Du, Q. Ma, L.-Z. Zhang, S.-J. Bao, X. Li, Y. Chen, M. Xu, *J. Mater. Chem. A* **2019**, *7*, 12276; c) B. Jin, L. Yang, J. Zhang, Y. Cai, J. Zhu, J. Lu, Y. Hou, Q. He, H. Xing, X. Zhan, F. Chen, Q. Zhang, *Adv. Energy Mater.* **2019**, *9*, 1902938.
- [7] a) C. Monroe, J. Newman, *J. Electrochem. Soc.* **2005**, *152*, A396; b) K. Fu, Y. Gong, B. Liu, Y. Zhu, S. Xu, Y. Yao, W. Luo, C. Wang, S. D. Lacey, J. Dai, Y. Chen, Y. Mo, E. Wachsman, L. Hu, *Sci. Adv.* **2017**, *3*, e1601659; c) X. Han, Y. Gong, K. Fu, X. He, G. T. Hitz, J. Dai, A. Pearse, B. Liu, H. Wang, G. Rubloff, Y. Mo, V. Thangadurai, E. D. Wachsman, L. Hu, *Nat. Mater.* **2017**, *16*, 572; d) Y. Li, W. Zhou, X. Chen, X. Lü, Z. Cui, S. Xin, L. Xue, Q. Jia, J. B. Goodenough, *Proc. Natl. Acad. Sci. USA* **2016**, *113*, 13313; e) W. Ling, N. Fu, J. Yue, X.-X. Zeng, Q. Ma, Q. Deng, Y. Xiao, L.-J. Wan, Y.-G. Guo, X.-W. Wu, *Adv. Energy Mater.* **2020**, *10*, 1903966; f) J. Zhang, C. Zheng, L. Li, Y. Xia, H. Huang, Y. Gan, C. Liang, X. He, X. Tao, W. Zhang, *Adv. Energy Mater.* **2020**, *10*, 2070017; g) K. Kaup, J. D. Bazak, S. H. Vajargah, X. Wu, J. Kulisch, G. R. Goward, L. F. Nazar, *Adv. Energy Mater.* **2020**, *10*, 1902783; h) T. Shi, Q. Tu, Y. Tian, Y. Xiao, L. J. Miara, O. Kononova, G. Ceder, *Adv. Energy Mater.* **2020**, *10*, 1902881; i) G. Chen, L. Ye, K. Zhang, M. Gao, H. Lu, H. Xu, Y. Bai, C. Wu, *Chem. Eng. J.* **2020**, *394*, 124885; j) C. Wu, S. Gu, Q. Zhang, Y. Bai, M. Li, Y. Yuan, H. Wang, X. Liu, Y. Yuan, N. Zhu, F. Wu, H. Li, L. Gu, J. Lu, *Nat. Commun.* **2019**, *10*, 73.
- [8] a) P. Gao, Z. Chen, Y. Gong, R. Zhang, H. Liu, P. Tang, X. Chen, S. Passerini, J. Liu, *Adv. Energy Mater.* **2020**, *10*, 1903780; b) S. Wei, C. Wang, S. Chen, P. Zhang, K. Zhu, C. Wu, P. Song, W. Wen, L. Song, *Adv. Energy Mater.* **2020**, *10*, 1903712; c) W. Li, C. Han, W. Wang, Q. Xia, S. Chou, Q. Gu, B. Johannessen, H. Liu, S. Dou, *Adv. Energy Mater.* **2020**, *10*, 1903006; d) S. Wang, X.-B. Zhang, *Adv. Mater.* **2019**, *31*, 1805432.
- [9] a) Q. Xu, T. Yang, W. Gao, R. Zhan, Y. Zhang, S. Bao, X. Li, Y. Chen, M. Xu, *J. Power Sources* **2019**, *443*, 227245; b) M. Jia, S. Lu, Y. Chen, T. Liu, J. Han, B. Shen, X. Wu, S.-J. Bao, J. Jiang, M. Xu, *J. Power Sources* **2017**, *367*, 17; c) L. Hu, J. Hou, F. Yi, Y. Chen, Y. Niu, J. Han, Y. Zhang, Z. Lu, M. Xu, *Electrochim. Acta* **2017**, *246*, 141; d) X. Shen, R. Zhang, X. Chen, X.-B. Cheng, X. Li, Q. Zhang, *Adv. Energy Mater.* **2020**, *10*, 1903645; e) Z. Wang, F. Qi, L. Yin, Y. Shi, C. Sun, B. An, H.-M. Cheng, F. Li, *Adv. Energy Mater.* **2020**, *10*, 1903843; f) Y. Wang, Y. Yu, Y. Tan, T. Li, Y. Chen, S. Wang, K. Sui, H. Zhang, Y. Luo, X. Li, *Adv. Energy Mater.* **2020**, *10*, 1903233.
- [10] a) X. Li, Y. Chen, J. Zou, X. Zeng, L. Zhou, H. Huang, *J. Power Sources* **2016**, *331*, 360; b) Y. Chen, C. Liu, X. Sun, H. Ye, C. Cheung, L. Zhou, *J. Power Sources* **2015**, *275*, 26; c) Y. Chen, Z. Lu, L. Zhou, Y.-W. Mai, H. Huang, *Nanoscale* **2012**, *4*, 6800; d) X. Chang, X. Zhou, X. Ou, C.-S. Lee, J. Zhou, Y. Tang, *Adv. Energy Mater.* **2019**, *9*, 1902672; e) X. Li, N. Fu, J. Zhou, X. Zeng, Y. Chen, L. Zhou, W. Lu, H. Huang, *Electrochim. Acta* **2017**, *225*, 137.
- [11] a) S. Fang, D. Bresser, S. Passerini, *Adv. Energy Mater.* **2020**, *10*, 1902485; b) X. Yu, H. Wu, J. H. Koo, A. Manthiram, *Adv. Energy Mater.* **2020**, *10*, 1902872.
- [12] a) Y. M. Chen, Z. Li, X. W. Lou, *Angew. Chem., Int. Ed.* **2015**, *54*, 10521; b) H. Chen, Y. Wu, J. Duan, R. Zhan, W. Wang, M.-Q. Wang, Y. Chen, M. Xu, S.-J. Bao, *ACS Appl. Mater. Interfaces* **2019**, *11*, 42197.
- [13] a) X. Li, Y. Chen, H. Huang, Y.-W. Mai, L. Zhou, *Energy Storage Mater.* **2016**, *5*, 58; b) Q. Ni, Y. Bai, Y. Li, L. Ling, L. Li, G. Chen, Z. Wang, H. Ren, F. Wu, C. Wu, *Small* **2018**, *14*, 1702864; c) Q. Ni, R. Dong, Y. Bai, Z. Wang, H. Ren, S. Sean, F. Wu, H. Xu, C. Wu, *Energy Storage Mater.* **2020**, *25*, 903; d) Q. Ni, Y. Bai, S. Guo, H. Ren, G. Chen, Z. Wang, F. Wu, C. Wu, *ACS Appl. Mater. Interfaces* **2019**, *11*, 5183.
- [14] a) Y. Chen, X. Li, X. Zhou, H. Yao, H. Huang, Y.-W. Mai, L. Zhou, *Energy Environ. Sci.* **2014**, *7*, 2689; b) Y. M. Chen, X. Y. Yu, Z. Li, U. Paik, X. W. Lou, *Sci. Adv.* **2016**, *2*, e1600021.
- [15] a) Y. Chen, J. Dong, L. Qiu, X. Li, Q. Li, H. Wang, S. Liang, H. Yao, H. Huang, H. Gao, J.-K. Kim, F. Ding, L. Zhou, *Chem* **2017**, *2*, 299; b) Y. Chen, Z. Wang, X. Li, X. Yao, C. Wang, Y. Li, W. Xue, D. Yu, S. Y. Kim, F. Yang, A. Kushima, G. Zhang, H. Huang, N. Wu, Y.-W. Mai, J. B. Goodenough, J. Li, *Nature* **2020**, *578*, 251.
- [16] a) Z. Zhou, B. Chen, T. Fang, Y. Li, Z. Zhou, Q. Wang, J. Zhang, Y. Zhao, *Adv. Energy Mater.* **2020**, *10*, 1902023; b) S. Agarwal, A. Greiner, *Polym. Adv. Technol.* **2011**, *22*, 372; c) L. M. Bellan, H. G. Craighead, *Polym. Adv. Technol.* **2011**, *22*, 304; d) M. Inagaki,

- Y. Yang, F. Kang, *Adv. Mater.* **2012**, *24*, 2547; e) X. Li, W. Yang, H. Li, Y. Wang, M. M. Bubakir, Y. Ding, Y. Zhang, *J. Appl. Polym. Sci.* **2015**, *132*, 41601; f) C. Pu, J. He, S. Cui, W. Gao, *J. Appl. Polym. Sci.* **2014**, *131*, 596; g) J. L. Shamshina, O. Zavgorodnya, J. R. Bonner, G. Gurau, T. Di Nardo, R. D. Rogers, *ChemSusChem* **2017**, *10*, 106; h) A. L. Yarin, *Polym. Adv. Technol.* **2011**, *22*, 310.
- [17] A. Formhals, *Google Patents*, **1934**.
- [18] a) T. Jin, Y. Liu, Y. Li, K. Cao, X. Wang, L. Jiao, *Adv. Energy Mater.* **2017**, *7*, 1700087; b) X. Lu, C. Wang, F. Favier, N. Pinna, *Adv. Energy Mater.* **2017**, *7*, 1601301; c) W. Xu, X. Hu, S. Zhuang, Y. Wang, X. Li, L. Zhou, S. Zhu, J. Zhu, *Adv. Energy Mater.* **2018**, *8*, 1702884; d) Y. Zhang, V. Srot, I. Moudrakovski, Y. Feng, P. A. van Aken, J. Maier, Y. Yu, *Adv. Energy Mater.* **2019**, *9*, 1901470.
- [19] X. Li, K. Li, S. Zhu, K. Fan, L. Lyu, H. Yao, Y. Li, J. Hu, H. Huang, Y.-W. Mai, J. B. Goodenough, *Angew. Chem., Int. Ed.* **2019**, *58*, 6239.
- [20] R. A. Thakur, C. A. Florek, J. Kohn, B. B. Michniak, *Int. J. Pharm.* **2008**, *364*, 87.
- [21] D. Li, M. W. Frey, A. J. Baeumner, *J. Membr. Sci.* **2006**, *279*, 354.
- [22] X.-H. Qin, S.-Y. Wang, *J. Appl. Polym. Sci.* **2006**, *102*, 1285.
- [23] L. Persano, A. Camposo, C. Tekmen, D. Pisignano, *Macromol. Mater. Eng.* **2013**, *298*, 504.
- [24] G. M. Bose, *Recherches sur la cause et sur la veritable theorie de l'electricite publies par George Mathias Bose prof. en phisique, de l'imprimerie de Jean Fred, Slomac 1745*.
- [25] G. I. Taylor, *Proc. R. Soc. London, Ser. A* **1964**, *280*, 383.
- [26] G. I. Taylor, M. D. Van Dyke, *Proc. R. Soc. London, Ser. A* **1969**, *313*, 453.
- [27] a) D. H. Reneker, A. L. Yarin, H. Fong, S. Koombhongse, *J. Appl. Phys.* **2000**, *87*, 4531; b) D. H. Reneker, A. L. Yarin, *Polymer* **2008**, *49*, 2387.
- [28] a) G. C. Rutledge, Y. Li, S. Fridrikh, S. B. Warner, V. E. Kalayci, P. Patra, *National Textile Center Annual Report M01*, **2001**; b) M. Y. Shin, M. M. Hohman, M. Brenner, G. C. Rutledge, *Appl. Phys. Lett.* **2001**, *78*, 1149; c) M. M. Hohman, Y. M. Shin, G. Rutledge, M. P. Brenner, *Phys. Fluids* **2001**, *13*, 2201.
- [29] S. V. Fridrikh, J. H. Yu, M. P. Brenner, G. C. Rutledge, *Phys. Rev. Lett.* **2003**, *90*, 144502.
- [30] G. Larsen, R. Velarde-Ortiz, K. Minchow, A. Barrero, I. G. Loscertales, *J. Am. Chem. Soc.* **2003**, *125*, 1154.
- [31] a) Y. Chen, Z. Lu, L. Zhou, Y.-W. Mai, H. Huang, *Energy Environ. Sci.* **2012**, *5*, 7898; b) Y. Yao, Z. Huang, P. Xie, S. Lacey, R. Jacob, H. Xie, F. Chen, A. Nie, T. Pu, M. Rehwoldt, D. Yu, M. Zachariah, C. Wang, R. Shahbazian-Yassar, J. Li, L. Hu, *Science* **2018**, *359*, 1489; c) P. Lu, D. Xie, B. Liu, F. Ai, Z. Zhang, M. Jin, X. Zhang, E. Ma, J. Li, Z. Shan, **2018**, arXiv:1802.00207.
- [32] a) S. De Vrieze, P. Westbroek, T. Van Camp, K. De Clerck, *J. Appl. Polym. Sci.* **2010**, *115*, 837; b) J. Fang, H. Wang, H. Niu, T. Lin, X. Wang, *J. Appl. Polym. Sci.* **2010**, *118*, 2553; c) A. S. Levitt, R. Vallett, G. Dion, C. L. Schauer, *J. Appl. Polym. Sci.* **2018**, *135*, 46404; d) Y. Liu, X. Li, S. Ramakrishna, *J. Polym. Sci., Part B: Polym. Phys.* **2014**, *52*, 946; e) X. Lu, C. Wang, Y. Wei, *Small* **2009**, *5*, 2349; f) X.-H. Qin, E.-L. Yang, N. Li, S.-Y. Wang, *J. Appl. Polym. Sci.* **2007**, *103*, 3865; g) A. Varesano, F. Rombaldoni, G. Mazzuchetti, C. Tonin, R. Comotto, *Polym. Int.* **2010**, *59*, 1606; h) G. Vasilyev, M. Burman, A. Arinstein, E. Zussman, *Macromol. Mater. Eng.* **2017**, *302*, 1600554; i) Y.-Q. Wan, J.-H. He, J.-Y. Yu, Y. Wu, *J. Appl. Polym. Sci.* **2007**, *103*, 3840; j) E. Yang, J. Shi, Y. Xue, *J. Appl. Polym. Sci.* **2010**, *116*, 3688.
- [33] a) A. Greiner, J. H. Wendorff, *Angew. Chem., Int. Ed.* **2007**, *46*, 5670; b) D. Li, Y. Xia, *Adv. Mater.* **2004**, *16*, 1151; c) H. Peng, Y. Liu, S. Ramakrishna, *J. Appl. Polym. Sci.* **2017**, *134*, 44578; d) S. Zhao, X. Wu, L. Wang, Y. Huang, *J. Appl. Polym. Sci.* **2004**, *91*, 242.
- [34] a) C. Berkland, D. W. Pack, K. Kim, *Biomaterials* **2004**, *25*, 5649; b) X. Wu, L. Wang, H. Yu, Y. Huang, *J. Appl. Polym. Sci.* **2005**, *97*, 1292.
- [35] T. Uyar, F. Besenbacher, *Polymer* **2008**, *49*, 5336.
- [36] C.-M. Hsu, S. Shivkumar, *Macromol. Mater. Eng.* **2004**, *289*, 334.
- [37] A. K. Haghi, M. Akbari, *Phys. Status Solidi A* **2007**, *204*, 1830.
- [38] J. Zeng, H. Hou, A. Schaper, J. H. Wendorff, A. Greiner, *e-Polymers* **2003**, *3*, 9.
- [39] N. Amiralayan, M. Nouri, M. H. Kish, *J. Appl. Polym. Sci.* **2009**, *113*, 226.
- [40] M. G. McKee, G. L. Wilkes, R. H. Colby, T. E. Long, *Macromolecules* **2004**, *37*, 1760.
- [41] a) J. Yoon, H.-S. Yang, B.-S. Lee, W.-R. Yu, *Adv. Mater.* **2018**, *30*, 1704765; b) J. Huang, Y. Lo, J. Niu, A. Kushima, X. Qian, L. Zhong, S. Mao, J. Li, *Nat. Nanotechnol.* **2013**, *8*, 277.
- [42] a) U. Boudriot, R. Dersch, A. Greiner, J. H. Wendorff, *Artif. Organs* **2006**, *30*, 785; b) V. Y. Chakrapani, A. Gnanamani, V. R. Giridev, M. Madhusoothanan, G. Sekaran, *J. Appl. Polym. Sci.* **2012**, *125*, 3221; c) T. Maeda, K. Takaesu, A. Hotta, *J. Appl. Polym. Sci.* **2016**, *133*, 43238.
- [43] C. L. Casper, J. S. Stephens, N. G. Tassi, D. B. Chase, J. F. Rabolt, *Macromolecules* **2004**, *37*, 573.
- [44] a) Y. Chen, Q. Qian, X. Liu, L. Xiao, Q. Chen, *Mater. Lett.* **2010**, *64*, 6; b) Q. Yang, Z. Li, Y. Hong, Y. Zhao, S. Qiu, C. Wang, Y. Wei, *J. Polym. Sci., Part B: Polym. Phys.* **2004**, *42*, 3721; c) T. Wang, S. Kumar, *J. Appl. Polym. Sci.* **2006**, *102*, 1023; d) N. Amini, S. Mazinani, S.-O. Ranaei-Siadat, M. Kalaei, K. Niknam, V. Adifar, *Fibers Polym.* **2012**, *13*, 994; e) Y. Zhang, T. X. Li, X. Ding, J. Y. Hu, X. D. Yang, *J. Donghua Univ.* **2014**, *31*, 511.
- [45] a) A. Baji, Y.-W. Mai, S.-C. Wong, M. Abtahi, P. Chen, *Compos. Sci. Technol.* **2010**, *70*, 703; b) S. Shenoy, W. Bates, H. Frisch, G. Wnek, *Polymer* **2005**, *46*, 3372.
- [46] a) K. Jensen, *J. Electrochem. Soc.* **1950**, **1983**, *130*; b) M. Moravej, R. F. Hicks, *Chem. Vapor. Deposition* **2005**, *11*, 469; c) U. Jansson, *Appl. Surf. Sci.* **1993**, *73*, 51.
- [47] a) H. Hou, D. H. Reneker, *Adv. Mater.* **2004**, *16*, 69; b) H. Wu, G. Chan, J. W. Choi, I. Ryu, Y. Yao, M. T. McDowell, S. W. Lee, A. Jackson, Y. Yang, L. Hu, Y. Cui, *Nat. Nanotechnol.* **2012**, *7*, 310; c) J. Plutnar, M. Pumera, Z. Sofer, *J. Mater. Chem. C* **2018**, *6*, 6082; d) S.-M. Yoon, W. M. Choi, H. Baik, H.-J. Shin, I. Song, M.-S. Kwon, J. J. Bae, H. Kim, Y. H. Lee, J.-Y. Choi, *ACS Nano* **2012**, *6*, 6803; e) W. Muangrat, W. Wongwiriyan, S. Morimoto, Y. Hashimoto, *Sci. Rep.* **2019**, *9*, 7871; f) S. Ullah, M. Hasan, H. Q. Ta, L. Zhao, Q. Shi, L. Fu, J. Choi, R. Yang, Z. Liu, M. H. Rummeli, *Adv. Funct. Mater.* **2019**, *29*, 1904457; g) Y. Liang, N. Li, F. Li, Z. Xu, Y. Hu, M. Jing, K. Teng, X. Yan, J. Shi, *Electrochim. Acta* **2019**, *297*, 1063; h) S. Liang, X. Pei, W. Jiang, Z. Xu, W. Wang, K. Teng, C. Wang, H. Fu, X. Zhang, *Electrochim. Acta* **2019**, *322*, 134696; i) Z. Xu, Y. Zeng, L. Wang, N. Li, C. Chen, C. Li, J. Li, H. Lv, L. Kuang, X. Tian, *J. Power Sources* **2017**, *356*, 18; j) W. Jiang, H. Wang, Z. Xu, N. Li, C. Chen, C. Li, J. Li, H. Lv, L. Kuang, X. Tian, *Chem. Eng. J.* **2018**, *335*, 954.
- [48] a) J. Wathanaarun, V. Pavarajarn, P. Supaphol, *Sci. Technol. Adv. Mater.* **2005**, *6*, 240; b) S. Zhan, D. Chen, X. Jiao, C. Tao, *J. Phys. Chem. B* **2006**, *110*, 11199.
- [49] M. A. Kanjwal, N. A. M. Barakat, F. A. Sheikh, S. J. Park, H. Y. Kim, *Macromol. Res.* **2010**, *18*, 233.
- [50] J. Zhou, M. Zhou, Z. Chen, Z. Zhang, C. Chen, R. Li, X. Gao, E. Xie, *Surf. Coat. Technol.* **2009**, *203*, 3219.
- [51] Y. Chen, X. Li, K. Park, J. Song, J. Hong, L. Zhou, Y.-W. Mai, H. Huang, J. B. Goodenough, *J. Am. Chem. Soc.* **2013**, *135*, 16280.
- [52] a) R. Anton, *Carbon* **2008**, *46*, 656; b) S. Helveg, C. López-Cartes, J. Sehested, P. L. Hansen, B. S. Clausen, J. R. Rostrup-Nielsen, F. Abild-Pedersen, J. K. Nørskov, *Nature* **2004**, *427*, 426.
- [53] a) H. Wang, S. Lu, Y. Chen, L. Han, J. Zhou, X. Wu, W. Qin, *J. Mater. Chem. A* **2015**, *3*, 23677; b) Y. Wang, W. Kang, D. Cao, M. Zhang, Z. Kang, Z. Xiao, R. Wang, D. Sun, *J. Mater. Chem. A* **2018**, *6*, 4776; c) Y. Zhang, N. Wang, P. Xue, Y. Liu, B. Tang, Z. Bai, S. Dou, *Chem. Eng. J.* **2018**, *343*, 512; d) Y. Zhao, Q. Pang, Y. Wei, L. Wei, Y. Ju, B. Zou, Y. Gao, G. Chen, *ChemSusChem* **2017**, *10*, 4778.

- [54] Y. M. Chen, L. Yu, X. W. Lou, *Angew. Chem., Int. Ed.* **2016**, *55*, 5990.
- [55] Y. Chen, X. Li, K. Park, L. Zhou, H. Huang, Y.-W. Mai, J. B. Goodenough, *Angew. Chem., Int. Ed.* **2016**, *55*, 15831.
- [56] Y. Chen, X. Li, K. Park, W. Lu, C. Wang, W. Xue, F. Yang, J. Zhou, L. Suo, T. Lin, H. Huang, J. Li, J. B. Goodenough, *Chem* **2017**, *3*, 152.
- [57] X. M. Lin, J. H. Chen, J. J. Fan, Y. Ma, P. Radjenovic, Q. C. Xu, L. Huang, S. Passerini, Z. Q. Tian, J. F. Li, *Adv. Energy Mater.* **2019**, *9*, 1902312.
- [58] Z. Li, J. T. Zhang, Y. M. Chen, J. Li, X. W. Lou, *Nat. Commun.* **2015**, *6*, 8850.
- [59] D. Tian, X. Song, M. Wang, X. Wu, Y. Qiu, B. Guan, X. Xu, L. Fan, N. Zhang, K. Sun, *Adv. Energy Mater.* **2019**, *9*, 1901940.
- [60] Y. Xiao, B. Han, Y. Zeng, S. S. Chi, X. Zeng, Z. Zheng, K. Xu, Y. Deng, *Adv. Energy Mater.* **2020**, *10*, 1903937.
- [61] a) Y. Chen, X. Li, K. S. Park, J. Hong, J. Song, L. Zhou, Y.-W. Mai, H. Huang, J. B. Goodenough, *J. Mater. Chem. A* **2014**, *2*, 10126; b) F. Wu, L. Shi, D. Mu, H. Xu, B. Wu, *Carbon* **2015**, *86*, 146.
- [62] L. Lin, F. Pei, J. Peng, A. Fu, J. Cui, X. Fang, N. Zheng, *Nano Energy* **2018**, *54*, 50.
- [63] J. S. Lee, W. Kim, J. Jang, A. Manthiram, *Adv. Energy Mater.* **2017**, *7*, 1601943.
- [64] Y. Wu, M. Gao, X. Li, Y. Liu, H. Pan, *J. Alloys Compd.* **2014**, *608*, 220.
- [65] a) L. Zeng, Y. Jiang, J. Xu, M. Wang, W. Li, Y. Yu, *Nanoscale* **2015**, *7*, 10940; b) M. Liu, N. Deng, J. Ju, L. Fan, L. Wang, Z. Li, H. Zhao, G. Yang, W. Kang, J. Yan, B. Cheng, *Adv. Funct. Mater.* **2019**, *29*, 1905467.
- [66] a) G.-C. Li, G.-R. Li, S.-H. Ye, X.-P. Gao, *Adv. Energy Mater.* **2012**, *2*, 1238; b) X. Song, T. Gao, S. Wang, Y. Bao, G. Chen, L.-X. Ding, H. Wang, *J. Power Sources* **2017**, *356*, 172.
- [67] a) L. Fan, H. L. Zhuang, K. Zhang, V. R. Cooper, Q. Li, Y. Lu, *Adv. Sci.* **2016**, *3*, 1600175; b) S. Xue, S. Yao, M. Jing, L. Zhu, X. Shen, T. Li, Z. YiLiu, *Electrochim. Acta* **2019**, *299*, 549; c) R. Zhuang, S. Yao, X. Shen, T. Li, S. Qin, J. Yang, *J. Mater. Sci.* **2019**, *54*, 4626.
- [68] N. Deng, J. Ju, J. Yan, X. Zhou, Q. Qin, K. Zhang, Y. Liang, Q. Li, W. Kang, B. Cheng, *ACS Appl. Mater. Interfaces* **2018**, *10*, 12626.
- [69] a) S. Kim, C. Jung, H. Kim, K. E. Thomas-Alyea, G. Yoon, B. Kim, M. E. Badding, Z. Song, J. Chang, J. Kim, D. Im, K. Kang, *Adv. Energy Mater.* **2020**, *10*, 1903993; b) W.-J. Chen, B.-Q. Li, C.-X. Zhao, M. Zhao, T.-Q. Yuan, R.-C. Sun, J.-Q. Huang, Q. Zhang, *Angew. Chem.* **2019**, <https://doi.org/10.1002/ange.201912701>.
- [70] a) Z. Peng, J. Song, L. Huai, H. Jia, B. Xiao, L. Zou, G. Zhu, A. Martinez, S. Roy, V. Murugesan, H. Lee, X. Ren, Q. Li, B. Liu, X. Li, D. Wang, W. Xu, J.-G. Zhang, *Adv. Energy Mater.* **2019**, *9*, 1901764; b) X.-R. Chen, B.-Q. Li, C. Zhu, R. Zhang, X.-B. Cheng, J.-Q. Huang, Q. Zhang, *Adv. Energy Mater.* **2019**, *9*, 1901932.
- [71] S. Huang, L. Tang, H. S. Najafabadi, S. Chen, Z. Ren, *Nano Energy* **2017**, *38*, 504.
- [72] J. Xiang, Y. Zhao, L. Yuan, C. Chen, Y. Shen, F. Hu, Z. Hao, J. Liu, B. Xu, Y. Huang, *Nano Energy* **2017**, *42*, 262.
- [73] C. Yang, Y. Yao, S. He, H. Xie, E. Hitz, L. Hu, *Adv. Mater.* **2017**, *29*, 1702714.
- [74] a) C. Li, B. Qin, Y. Zhang, A. Varzi, S. Passerini, J. Wang, J. Dong, D. Zeng, Z. Liu, H. Cheng, *Adv. Energy Mater.* **2019**, *9*, 1803422; b) J. Wu, Z. Rao, Z. Cheng, L. Yuan, Z. Li, Y. Huang, *Adv. Energy Mater.* **2019**, *9*, 1902767.
- [75] X. Wang, Y. Zhang, X. Zhang, T. Liu, Y.-H. Lin, L. Li, Y. Shen, C.-W. Nan, *ACS Appl. Mater. Interfaces* **2018**, *10*, 24791.
- [76] S. Li, S.-Q. Zhang, L. Shen, Q. Liu, J.-B. Ma, W. Lv, Y.-B. He, Q.-H. Yang, *Adv. Sci.* **2020**, *7*, 1903088.
- [77] W. Liu, N. Liu, J. Sun, P.-C. Hsu, Y. Li, H.-W. Lee, Y. Cui, *Nano Lett.* **2015**, *15*, 2740.
- [78] K. Fu, Y. Gong, J. Dai, A. Gong, X. Han, Y. Yao, C. Wang, Y. Wang, Y. Chen, C. Yan, Y. Li, E. D. Wachsman, L. Hu, *Proc. Natl. Acad. Sci. USA* **2016**, *113*, 7094.
- [79] a) M. R. Khan, S. Harp, J. Neumann, Q. N. Sultana, *J. Mater. Eng. Perform.* **2016**, *25*, 1276; b) P. Zhu, J. Zhu, J. Zang, C. Chen, Y. Lu, M. Jiang, C. Yan, M. Dirican, R. Kalai Selvan, X. Zhang, *J. Mater. Chem. A* **2017**, *5*, 15096; c) L. Wang, N. Deng, L. Fan, L. Wang, G. Wang, W. Kang, B. Cheng, *Mater. Lett.* **2018**, *233*, 224.
- [80] M. Zhao, H.-J. Peng, J.-Y. Wei, J.-Q. Huang, B.-Q. Li, H. Yuan, Q. Zhang, *Small Methods* **2019**, 1900344.
- [81] N. Deng, W. Kang, Y. Liu, J. Ju, D. Wu, L. Li, B. S. Hassan, B. Cheng, *J. Power Sources* **2016**, *331*, 132.
- [82] a) J.-Q. Huang, T.-Z. Zhuang, Q. Zhang, H.-J. Peng, C.-M. Chen, F. Wei, *ACS Nano* **2015**, *9*, 3002; b) J. Zhu, E. Yildirim, K. Aly, J. Shen, C. Chen, Y. Lu, M. Jiang, D. Kim, A. E. Tonelli, M. A. Pasquinnelli, P. D. Bradford, X. Zhang, *J. Mater. Chem. A* **2016**, *4*, 13572.
- [83] a) K. Gao, X. Hu, C. Dai, T. Yi, *Mater. Sci. Eng., B* **2006**, *131*, 100; b) S. W. Choi, J. R. Kim, Y. R. Ahn, S. M. Jo, E. J. Cairns, *Chem. Mater.* **2007**, *19*, 104.
- [84] T. Lei, W. Chen, Y. Hu, W. Lv, X. Lv, Y. Yan, J. Huang, Y. Jiao, J. Chu, C. Yan, C. Wu, Q. Li, W. He, J. Xiong, *Adv. Energy Mater.* **2018**, *8*, 1802441.
- [85] B. Sun, Y.-Z. Long, Z.-J. Chen, S.-L. Liu, H.-D. Zhang, J.-C. Zhang, W.-P. Han, *J. Mater. Chem. C* **2014**, *2*, 1209.
- [86] a) S. Liu, Z. Wang, C. Yu, H. B. Wu, G. Wang, Q. Dong, J. Qiu, A. Eychmüller, X. W. Lou, *Adv. Mater.* **2013**, *25*, 3462; b) J. Liang, X. Gao, J. Guo, C. Chen, K. Fan, J. Ma, *Sci. China Mater.* **2018**, *61*, 30; c) X. Xiong, W. Luo, X. Hu, C. Chen, L. Qie, D. Hou, Y. Huang, *Sci. Rep.* **2015**, *5*, 9254.
- [87] a) C.-M. Wang, W. Xu, J. Liu, J.-G. Zhang, L. V. Saraf, B. W. Arey, D. Choi, Z.-G. Yang, J. Xiao, S. Thevuthasan, D. R. Baer, *Nano Lett.* **2011**, *11*, 1874; b) Z. Wang, P. Poncharal, W. de Heer, *J. Phys. Chem. Solids* **2000**, *61*, 1025; c) D. Qian, E. C. Dickey, *J. Microscopy* **2001**, *204*, 39.
- [88] D. J. Johnson, *J. Phys. D: Appl. Phys.* **1987**, *20*, 286.
- [89] S. M. Saufi, A. F. Ismail, *Songklanakarin J. Sci. Technol.* **2002**, *24*, 843.
- [90] M. S. A. Rahaman, A. F. Ismail, A. Mustafa, *Polym. Degrad. Stab.* **2007**, *92*, 1421.
- [91] S. Prilutsky, E. Zussman, Y. Cohen, *J. Polym. Sci., Part B: Polym. Phys.* **2010**, *48*, 2121.
- [92] a) F. Yang, X. Wang, D. Zhang, J. Yang, D. Luo, Z. Xu, J. Wei, J.-Q. Wang, Z. Xu, F. Peng, X. Li, R. Li, Y. Li, M. Li, X. Bai, F. Ding, Y. Li, *Nature* **2014**, *510*, 522; b) S. J. Yang, J. Y. Choi, H. K. Chae, J. H. Cho, K. S. Nahm, C. R. Park, *Chem. Mater.* **2009**, *21*, 1893.
- [93] a) Z. Wen, S. Ci, Y. Hou, J. Chen, *Angew. Chem., Int. Ed.* **2014**, *53*, 6496; b) S. Yasuda, T. Hiraoka, D. N. Futaba, T. Yamada, M. Yumura, K. Hata, *Nano Lett.* **2009**, *9*, 769.
- [94] M. Diarra, A. Zappelli, H. Amara, F. Ducastelle, C. Bichara, *Phys. Rev. Lett.* **2012**, *109*, 185501.
- [95] Q. Yuan, Z. Xu, B. I. Yakobson, F. Ding, *Phys. Rev. Lett.* **2012**, *108*, 245505.
- [96] C. M. Wang, W. Xu, J. Liu, D. W. Choi, B. Arey, L. V. Saraf, J. G. Zhang, Z. G. Yang, S. Thevuthasan, D. R. Baer, N. Salmon, *J. Mater. Res.* **2010**, *25*, 1541.
- [97] X. H. Liu, J. Y. Huang, *Energy Environ. Sci.* **2011**, *4*, 3844.
- [98] a) X. Zhou, L.-J. Wan, Y.-G. Guo, *Small* **2013**, *9*, 2684; b) T. H. Hwang, Y. M. Lee, B.-S. Kong, J.-S. Seo, J. W. Choi, *Nano Lett.* **2012**, *12*, 802.
- [99] M. Gu, Y. Li, X. Li, S. Hu, X. Zhang, W. Xu, S. Thevuthasan, D. R. Baer, J.-G. Zhang, J. Liu, C. Wang, *ACS Nano* **2012**, *6*, 8439.
- [100] X. Li, Y. Chen, H. Wang, H. Yao, H. Huang, Y.-W. Mai, N. Hu, L. Zhou, *Adv. Funct. Mater.* **2016**, *26*, 376.
- [101] Z.-L. Xu, J.-Q. Huang, W. G. Chong, X. Qin, X. Wang, L. Zhou, J.-K. Kim, *Adv. Energy Mater.* **2017**, *7*, 1602078.
- [102] Y. Li, Y. Li, A. Pei, K. Yan, Y. Sun, C.-L. Wu, L.-M. Joubert, R. Chin, A. L. Koh, Y. Yu, J. Perrino, B. Butz, S. Chu, Y. Cui, *Science* **2017**, *358*, 506.